

RESEARCH ARTICLE

Epigenetic control of region-specific transcriptional programs in mouse cerebellar and cortical astrocytes

Anna Welle¹  | Carmen V. Kasakow² | Annemarie M. Jungmann¹  |
Davide Gobbo²  | Laura Stopper² | Karl Nordström¹  |
Abdulrahman Salhab¹  | Gilles Gasparoni¹  | Anja Scheller²  |
Frank Kirchhoff²  | Jörn Walter¹ 

¹Department of Genetics and EpiGenetics, University of Saarland, Saarbrücken, Germany

²Molecular Physiology, Center for Integrative Physiology and Molecular Medicine, University of Saarland, Homburg, Germany

Correspondence

Jörn Walter, Department of Genetics and EpiGenetics, Universität des Saarlandes Campus A2 4, Saarbrücken 66123, Germany. Email: j.walter@mx.uni-saarland.de

Funding information

Bundesministerium für Bildung und Forschung, Grant/Award Numbers: 01KU1216F, 031L0101D, ERANET Neuron BrIE; Deutsche Forschungsgemeinschaft, Grant/Award Numbers: SFB 894, SPP 1757

Abstract

Astrocytes from the cerebral cortex (CTX) and cerebellum (CB) share basic molecular programs, but also form distinct spatial and functional subtypes. The regulatory epigenetic layers controlling such regional diversity have not been comprehensively investigated so far. Here, we present an integrated epigenome analysis of methylomes, open chromatin, and transcriptomes of astroglia populations isolated from the cortex or cerebellum of young adult mice. Besides a basic overall similarity in their epigenomic programs, cortical astrocytes and cerebellar astrocytes exhibit substantial differences in their overall open chromatin structure and in gene-specific DNA methylation. Regional epigenetic differences are linked to differences in transcriptional programs encompassing genes of region-specific transcription factor networks centered around *Lhx2/Foxg1* in CTX astrocytes and the *Zic/Irx* families in CB astrocytes. The distinct epigenetic signatures around these transcription factor networks point to a complex interconnected and combinatorial regulation of region-specific transcriptomes. These findings suggest that key transcription factors, previously linked to temporal, regional, and spatial control of neurogenesis, also form combinatorial networks important for astrocytes. Our study provides a valuable resource for the molecular basis of regional astrocyte identity and physiology.

KEYWORDS

astrocytes, chromatin accessibility, development, DNA methylation, epigenetics, gene expression, regionalization

1 | INTRODUCTION

For a long time, astrocytes were viewed as a functional homogenous cell population existing to support neurons throughout the brain. However, in the past decade the functional diversity of astrocytes in distinct brain regions became evident (reviewed by Farmer &

Murai, 2017 and Clarke, Taha, Tyzack, & Patani, 2021). It was demonstrated that gene expression changed gradually along the dorsoventral as well as the rostrocaudal axis of the brain (Borggrewe et al., 2020; Morel et al., 2017). Moreover, striatal and hippocampal astrocytes have specialized properties like altered morphology, electrophysiology, and Ca^{2+} -signaling within neural circuits (Chai et al., 2017). Distinct

This is an open access article under the terms of the Creative Commons Attribution-NonCommercial License, which permits use, distribution and reproduction in any medium, provided the original work is properly cited and is not used for commercial purposes.

© 2021 The Authors. *GLIA* published by Wiley Periodicals LLC.

astrocyte subtypes can be isolated based on GLAST expression from the forebrain, hindbrain, or spinal cord (Borggrewe et al., 2020). Along with distinct GLAST expression these astrocyte subtypes differ in their transcriptional programs and responsiveness during experimental autoimmune encephalomyelitis reflecting interregional and intraregional heterogeneity. The molecular heterogeneity of intraregional subpopulations is highly dependent on the interaction with the neuronal environment. Disruption of neuronal layers in the neocortex subsequently leads to the loss of layer-specific properties of cortical astrocytes (Lanjakornsiripan et al., 2018). In the cerebellum, neuron-derived sonic hedgehog (Shh) controls the gene expression profile of Bergmann glia, the astroglia of the cerebellar cortex, and is expected to drive the switch from velate astrocytes, located in the inner granular layer, toward Bergmann glia expression profiles (Farmer et al., 2016).

The regulatory mechanisms underlying the regional specification of astrocytes remain to be uncovered. Epigenetic modifications are strong potential candidates with their ability to establish and maintain cell identity by modulating gene expression. The genome-wide distribution of DNA methylation and its local variation is a good approximation to locate functional and cell-specific program changes in the genome. In addition, DNA methylation profiles allow to indirectly infer the developmental history of cells by using genome-wide DNA methylation comparisons (Durek et al., 2016; Salhab et al., 2018). Next to DNA methylation, chromatin modifications are excellent indicators of the functional state of genes and genomes. Both the dynamic changes in DNA methylation and the open chromatin signatures can be precisely mapped on isolated cells using genome-wide next generation sequencing (NGS) based approaches. DNA methylation and open chromatin maps allow comprehensive identification of the functional changes at regulatory regions linked to a different spatial or temporal origin of cells. The integrated analysis of epigenetic modifications at promoters and other putative distal or proximal *cis* regulatory regions helps to understand the regulatory programs of astroglial populations from different brain regions to (a) identify commonalities referring to their developmental origin and (b) identify differences explaining their functional, epigenomic, and regional diversity.

In this study, we analyzed the molecular diversity of GFAP-EGFP-positive astrocytes from two distinct adult brain regions (protoplasmic astrocytes from the cerebral cortex and mainly Bergmann glia from the cerebellum; for simplicity we refer to them as CTX and CB astrocytes) by an integrative genome-wide approach using comprehensive epigenomic and gene expression profiling. Our analysis highlights the principle of inherited regional specification and diversification by interaction with distinct environment in the respective brain regions.

2 | MATERIALS AND METHODS

2.1 | Contact for reagent and resource sharing

Further information and requests for resources and reagents should be directed to, and will be fulfilled by, the Lead Contact, Jörn Walter (j.walter@mx.uni-saarland.de).

2.2 | Experimental model and subject details

Animal experiments were carried out at the University of Saarland according to European and German guidelines and approved by “Landesamt für Gesundheit und Verbraucherschutz” of the state of Saarland (license: perfusion [C1-2.4.7.1]). Transgenic heterozygous TgN(hGFAP-EGFP)_{GFEA} (hGFAP-EGFP; Nolte et al., 2001) and TgN(PLP-DsRed1)_{PRDB} (PLP-DsRed1) mice (Hirrlinger et al., 2005) were maintained in the animal facility of the CIPMM, were generally fed a breeding diet (V1125, Ssniff) ad libitum and were held at a 12-h light/dark cycle. Mice were bred in FVB/N background to keep a stable and strong transgene expression under control of the human GFAP promoter (Bai et al., 2013). For NeuN-based FACSorting 6-week-old F1(C57BL6/J x DBA2/N) mice were used. Male and female mice were used for the experiments, sex chromosomes were excluded from the analyses.

2.3 | Cell type enrichment

Isolation of astrocytes was performed as described previously (Lovatt et al., 2007; Orre et al., 2014) with few modifications. hGFAP-EGFP single transgenic (6 weeks old) mice were perfused with HBSS (Sigma Aldrich), decapitated and the brain was dissected into cerebellum and cerebral cortex. For each experiment the brains of two mice were used to achieve the desired cell yield. Tissue was minced and washed with HBSS and PIPES working solution (0.5 M PIPES stock buffer (PIPES 0.5 M (Sigma Aldrich), 1 M NaOH, 1.2 M NaCl, and 50 mM KCl solution, 45% glucose in 50 ml ddH₂O) followed by 50 min digestion with activated papain (156 µl of 16 U/ml papain (Sigma Aldrich), 500 µl of Papain activation buffer: 55 mM L-Cystein HCl, 11 mM EDTA, pH 7.4; 4.5 ml PIPES working solution) and DNase I (80 Kunitz units/ml, Sigma Aldrich) at 37°C and low speed rotation. The tissue was gently triturated by 5–10 strokes with a P1000 pipette, DNase I solution (100 µl DNase I in 3 ml wash media [DMEM, 0.5% BSA] to a final concentration 25 Kunitz units/ml) was added and the digestion was carried out for 15 min at 37°C with low speed rotation. The tissue was triturated into a single cell suspension, filtered through a 70 µm strainer (Greiner) and washed with 40 ml washing media. Cells were resuspended in GKN buffer (80 g/L NaCl, 4 g/L KCl, 35.6 g/L Na₂HPO₄ 12 H₂O, 7.8 g/L NaH₂PO₄·2 H₂O, 20 g/L D-(+)-glucose, pH 7.4) and sorted with a FACS Aria III (Becton Dickinson) based on Hoechst blue (Sigma Aldrich) and EGFP fluorescence signals. Cells were sorted into 250 µl GKN buffer and pelleted at 500g, 4°C, for 10 min. The supernatant was discarded and the pellet was frozen at –80°C for RRBS and mRNA-Seq library preparation. hGFAP-EGFP x PLP-DsRed1 double transgenic mice were used to isolate oligodendrocytes following the procedures described above and sorted based on Hoechst blue and DsRed fluorescence. Neuronal and non-neuronal nuclei of F1(C57BL6/J x DBA2/N) mice were extracted from frozen forebrain tissue using a protocol previously described (Matevosian & Akbarian, 2008) with essential modifications. The tissue was dissociated using a Dounce tissue grinder placed on ice with 50 strokes in

5 ml homogenization buffer (10 mM Tris-HCl (pH 8), 0.1 mM EDTA, 3 mM Mg(Ac)₂, 5 mM CaCl₂, 0.1% NP-40, 0.32 M sucrose, 1× cOmplete EDTA-free Protease Inhibitor Cocktail (Sigma Aldrich), 0.16 mM DTT, 10 mM PMSF). Nuclei suspension was filtered through a 150 μm strainer followed by a 20 μm strainer (CellTrics, Symex Partec) to remove nondissociated tissue. Additional, cell debris removal was carried out by centrifugation in 25% Percoll solution (Sigma Aldrich) for 15 min at 4°C with 750g and low brake. Nuclei were washed with phosphate buffered saline (PBS; pH 7.4) supplemented with 1× cOmplete, EDTA-free Protease Inhibitor Cocktail and kept in blocking solution (3% bovine serum albumin, 2% normal goat serum in 1× PBS; pH 7.4) for 30 min at 4°C. Anti-NeuN-Alexa488 antibody (MAB377X; Merck) was diluted 1:1,000 in the same volume of blocking solution as the nuclei. Nuclei and antibodies were mixed and kept at 4°C in the dark for 1 hr. After removal of antibody solution, nuclei were resuspended in blocking solution supplemented with 1 μg/ml propidium iodide (PI; Miltenyi Biotec). Sorting gates were set based on PI and Alexa488 signal intensities. Nuclei were pelleted and kept frozen at -80°C for RRBS or used directly for ATAC-Seq library preparation.

2.4 | Preparation of mRNA-Seq libraries

Frozen pellets of 10⁵ cells were used for mRNA capturing using mRNA Capture Kit (Roche) with minor modifications. Cells were lysed in 49 μl lysis buffer and 1 μl of the biotinylated oligo(dT)₂₀ working solution was added to the lysate. Lysate was transferred into streptavidin coated tubes to immobilize the mRNA. M-MLV Reverse Transcriptase RNase H⁻ (400 U; Promega) in 50 μl reaction volume was used for first strand synthesis at 37°C for 1 hr. Second strand synthesis was carried out at 16°C for 2.5 hr using 400 U T4-Ligase, 5 U RNase H and 50 U DNA Polymearse I (New England Biolabs). The sequencing libraries were prepared with the Nextera DNA Library Preparation Kit (Illumina) with 0.2 μl of the Tagment DNA Enzyme 1 in a 50 μl reaction at 55°C for 5 min followed by purification of the DNA using MinElute PCR Purification Kit (Qiagen) following the manufacturer's protocol. Library amplification was done by 12 cycles of PCR with the NEBNext High-Fidelity 2X PCR Master Mix (New England Biolabs) using 0.2 μM Index-adapters (5'-AAT GAT ACG GCG ACC ACC GAG ATC TAC AC [i5] TCG TCG GCA GCG TC-3' and 5'-CAA GCA GAA GAC GGC ATA CGA GAT [i7] GT CTC GTG GGC TCG G-3'; Illumina). The libraries were purified with 0.8× Agencourt AMPure XP (Beckman Coulter) and sequenced on the Illumina HiSeq 2500 with 1 × 100 bp single-end reads.

2.5 | Preparation of ATAC-Seq libraries

For ATAC the cell pellet of 5 × 10⁴ cells was carefully resuspended in nuclei extraction buffer (60 mM KCl, 15 mM Tris-HCl, 15 mM NaCl, 1 mM EDTA, 0.5 mM EGTA, 0.5 mM spermidine [free base], 1X

cOmplete Protease Inhibitor Cocktail, 0.1% NP-40), kept on ice for 10 min and centrifuged at 500g, 4°C, for 10 min. The supernatant was discarded and the nuclei were carefully resuspended in 50 μl ATAC reaction buffer (1X Illumina Tagment DNA Buffer, 2.5 μl Illumina Tagment DNA Enzyme). The reaction was incubated at 37°C for 30 min followed by DNA purification (MinElute PCR Purification Kit; Qiagen). Library amplification was carried out using the NEBNext High-Fidelity 2X PCR Master Mix (New England Biolabs) using 0.2 μM Index-adapters (5'-AAT GAT ACG GCG ACC ACC GAG ATC TAC AC [i5] TCG TCG GCA GCG TC-3' and 5'-CAA GCA GAA GAC GGC ATA CGA GAT [i7] GT CTC GTG GGC TCG G-3'; Illumina) with 10 cycles of PCR. The libraries were purified with 1× Agencourt AMPure XP (Beckman Coulter) and sequenced on the Illumina HiSeq 2500 with 2 × 100 bp paired-end reads.

2.6 | Preparation of RRBS libraries

Sorted cells were lysed, digested with proteinase K and protease activity was inhibited by Pefabloc SC (1 mM; Sigma-Aldrich). DNA of the lysates was *HaellI*-digested overnight (50 U; New England Biolabs) and inactivated at 80°C. A-tailing was performed using Klenow exo⁻ (5 U; New England Biolabs) at 37°C for 30 min. TruSeq DNA Single Indexes Set A adapters (1:10 dilution; Illumina) were ligated at 16°C overnight using T4-Ligase (2,000 U; New England Biolabs). Before bisulfite conversion (EZ DNA Methylation-Gold Kit; Zymo research) adapter ligated DNA fragments were purified with 1.5× Agencourt AMPure XP (Beckman Coulter). Purified adapter ligated DNA fragments were amplified by 14–15 cycles of PCR using HotStarTaq DNA Polymearse (Qiagen) and PCR primers (5'-AAT GAT ACG GCG ACC ACC GAG ATC TAC AC-3' and 5'-CAA GCA GAA GAC GGC ATA CGA GAT-3' and size selected using 0.9× Agencourt AMPure XP (Beckman Coulter). Library size distribution was assessed using the Agilent 2100 Bioanalyzer and library concentrations were measured using Qubit[®] dsDNA HS Assay Kit (Thermo Fisher Scientific) before sequencing on the Illumina HiSeq 2500 with 100 bp single-end reads. The samples CB2, CTX4, and Oligodendrocytes were sequenced with 90 bp single-end reads.

2.7 | mRNA-Seq data analysis

FastQ format reads were trimmed for adapter sequences and low-quality ends (phred score <20) using Trim Galore! (http://www.bioinformatics.babraham.ac.uk/projects/trim_galore/; version 0.4.2). 2-step STAR alignment (Dobin & Gingeras, 2015) method was used to align the reads to the mm10 reference genome. PCR duplications were marked using MarkDuplicate from Picard tools (version 1.115; <http://broadinstitute.github.io/picard/>) followed by quality control using RNA-seQC (DeLuca et al., 2012). Mapped reads were assigned to genes from Gencode annotation (vM2; <https://www.encodeproject.org/files/gencode.vM2.annotation>) using featureCounts (Liao, Smyth, & Shi, 2014). Read counts were analyzed using the R package edgeR

(M. D. Robinson, McCarthy, & Smyth, 2010). The counts were filtered for $\text{cpm} \geq 2.5$ in at least two samples of a group. The data were normalized with the trimmed mean of M-values (TMM) method using the *calcNormFactors* function. Estimation of dispersion was done using *estimateDisp* and a generalized linear model was fit using *glmQLFit*. Differential expression defined by statistical cutoffs of p -value ≤ 0.01 and an FDR ≤ 0.05 . Correlation between the expression values of the data in this study with published data was calculated using the R function *cor* which returns Pearson coefficients. GO term enrichment was performed using DAVID functional annotation (Huang, Sherman, & Lempicki, 2009a, 2009b). The reduced visualization of GO terms was done with REVIGO (Supek, Bošnjak, Škunca, & Šmuc, 2011). Heatmaps of row-Z-scores were generated using the R package *pheatmap* (<https://CRAN.R-project.org/package=pheatmap>).

2.8 | ATAC-Seq data analysis

Low quality read tails ($Q < 20$) and adapter sequence were trimmed using Trim Galore (version 0.4.2; http://www.bioinformatics.babraham.ac.uk/projects/trim_galore). Trimmed reads were aligned to the mouse reference genome (mm10) using GEM mapper (version 1.376 beta; Marco-Sola, Sammeth, Guigó, & Ribeca, 2012). samtools (version 1.3; Li et al., 2009) was used to convert SAM to BAM format. MarkDuplicate (version 1.115) from Picard tools (<http://broadinstitute.github.io/picard/>) was used to mark the PCR duplications. Peaks were called using macs2 (version 2.1.0.20140616; Zhang et al., 2008) with the following parameters: `-nomodel, -shift -125, -extsize 250`. Normalized coverage files with respect to library size were generated using deepTools v1.5.9.1 (Ramírez, Dündar, Diehl, Grüning, & Manke, 2014) with *bamCoverage* command. Heatmaps were generated using deepTools *computeMatrix* command with center of region as reference point and 1,000 bp upstream and downstream distances. Coverage profiles were generated using the deepTools *plotProfile* command. featureCounts (Liao et al., 2014) was used to count reads in 100 bp and 10 kb windows to subsequently perform differential analysis using the R package csaw (Lun & Smyth, 2016) with the following settings: 10 kb counts and 100 bp counts were used for normalization with the TMM method using the *normOffsets* wrapper function; windows with fold change > 2 above the background were kept using *filterWindows*; *estimateDisp* was used to estimate the dispersion and *glmQLFit* was used to fit a generalized linear model; differential enrichment was tested with the *glmQLFTest* command and adjacent or overlapping windows were merged into clusters up to 3 kb width with gaps no greater than 150 bp using *mergeWindows*; p -values were combined across clustered tests using *combineTests* to control the cluster FDR. Annotation of peaks and DARs to genes and genomic location was done using ChipSeek (Chen et al., 2014). Overrepresentation of transcription factor binding motifs were analyzed using RSAT (Nguyen et al., 2018). For the comparison of the ATAC-Seq data with published ChIP-Seq data, macs2 was used to call peaks for all data sets.

2.9 | RRBS data analysis

Trimming of RRBS data was performed with the Cutadapt (Martin, 2011) wrapper Trim Galore! in RRBS mode. Mapping to the mm10 reference genome using MethylCtools (Hovestadt et al., 2014) and DNA methylation calling were performed as described before (Durek et al., 2016). Analysis of the DNA methylation was carried out using the R package methylKit (Akalin et al., 2012) with filtering of CpGs for coverage $\geq 10\times$ using the *filterByCoverage* command and presence in at least three samples of a group with the *unite* function. Regions for differential test were defined as nonoverlapping 1 kb intervals covering ≥ 3 CpG sites with the *tileMethylCounts* command. *calculateDiffMeth* was used to test for differential methylation and DMRs were defined as regions with $\geq 25\%$ methylation difference between the cell types with q -value ≤ 0.01 . Annotation of DMRs to genes and genomic location was done using ChipSeek (Chen et al., 2014). The GO term enrichment for most variable CpGs was performed using GREAT (McLean et al., 2010). Overrepresentation of transcription factor binding motifs were analyzed using RSAT (Nguyen et al., 2018). Heatmaps were generated using the R package *pheatmap* (<https://CRAN.R-project.org/package=pheatmap>). The segmentation of the RRBS data was done as described previously (Salhab et al., 2018) using MethylSeekR (Burger, Gaidatzis, Schübeler, & Stadler, 2013) with default parameters. The partially methylated domains were further used to identify combinatorial patterns using the ChromH3M workflow (Salhab et al., 2018).

2.10 | Genome browser visualization

The data is represented in the genome browser IGV (J. T. Robinson et al., 2011; Thorvaldsdottir, Robinson, & Mesirov, 2013). Biological replicates were merged into one track using the function *Overlay Tracks*. Black bars mark covered CpG position. The represented CpG positions have coverage of $\geq 10\times$.

2.11 | Integrative analysis

For the pairwise comparison, DMRs and DARs were intersected based on the genomic position with an overlap of at least 1 bp using the command *intersect* from Galaxy (Afgan et al., 2018) Operation Tools (<https://github.com/galaxyproject/gops>). The correlation of gene expression and DMRs/DARs was done based on the gene symbol. The overlap of DARs, DMRs, and DEGs (Figure 4a) was done using the online tool *genevenn* (<http://genevenn.sourceforge.net/>). The GO term enrichment for DAR/DMR associated genes was performed using DAVID functional annotation (Huang et al., 2009a, 2009b) and Pantherdb (Mi et al., 2017; Mi, Muruganujan, Casagrande, & Thomas, 2013) was used for protein classification. The network analysis was done loading higher expressed transcription factors for each brain region into the STRING database (Szklarczyk et al., 2017). The network was imported and extended with the epigenetic information

in Cytoscape (Shannon et al., 2003). Heatmaps were generated using the R package *heatmap* (<https://CRAN.R-project.org/package=heatmap>). The underlying matrix was generated by first, intersecting DMRs with DARs by at least 1 bp overlap using the Galaxy *intersect* command, then expression of the genes annotated to the respective regions were retrieved. The row-Z-score was calculated on RRBS, mRNA-Seq, and ATAC-Seq data separately using the DNA methylation, RPKM, and cpm values, respectively. Each z-score table was joined by the chromosomal position and gene name, so that each row represents the values of a DMR overlapping with a DAR and the respective gene expression. The rows were clustered using Manhattan distance and average linkage.

2.12 | Immunohistochemistry

hGFAP-EGFP mice were anesthetized (ketamine/xylazine 140 mg/kg and 10 mg/kg body weight) and intracardially perfused with PBS and subsequently with 4% formaldehyde in 0.1 M phosphate buffer (pH 7.4). The brain was prepared and postfixed overnight. Sagittal slices were prepared with a vibratome (Leica VT1000S) and further processed for antibody staining as described previously (Jahn et al., 2018). Briefly, slices were incubated for permeabilization and blocking, followed by first antibody staining overnight at 4°C. After washing steps, slices were incubated with second antibody and DAPI (Roche) and mounted with ImmMount (Thermo Scientific). The following antibodies were used: rabbit anti-Lhx2 (1:500, Merck, ABE1402), goat anti-Zic1 (1:30, RDSsystems, AF4978), mouse anti-trimethyl Histone H3 (Lys27; 1:500, Millipore, 05-1951), rabbit anti-H3K27ac (1:500, Diagenode, C15410194), rabbit anti-H2A.Z (1:1,000, Active Motif, Cat No. 39943-39944, Lot No. 00913003). They were combined with the following secondary antibodies: donkey anti-rabbit (1:1,000) conjugated with Alexa 546 (Invitrogen, A10040), donkey anti-goat (1:1,000) conjugated with Alexa 555 (Invitrogen, A21432), donkey anti-mouse (1:1,000) conjugated with Alexa 555 (Invitrogen, A31570), goat anti-rabbit (1:200) conjugated with Abberior® STAR RED (Abberior Instruments, STRED-1002). Nuclei were stained with TO-PRO-3 (1:1,000, Invitrogen, T3605).

2.13 | Microscopic analysis and quantification

Epifluorescent images were collected by a fully automated slide scanner (AxioScan.Z1, Zeiss, Jena, Germany) equipped with an LED Light Source (Colibri 7, Zeiss, Jena, Germany; Huang, Bai, et al., 2020). The appropriate excitation and emission filters (excitation/emission wavelengths in nm) were set as: 353/465 (DAPI), 488/509 (green), 548/561 (red), and 650/673 (infrared). A Plan-Apochromat 10 ×/0.45 objective for pre-focusing and a Plan-Apochromat 20 ×/0.8 objective for fine focus image acquisition was used. Offline image stitching (8 μm stacks, variance projection) for overviews of brain slices and further analysis was performed using ZEN software (Blue Edition, Zeiss, Oberkochen, Germany).

Confocal images were recorded by laser scanning microscopy (LSM 710, Zeiss) using an argon-ion laser (488 nm) and helium neon lasers (543 nm, 633 nm), appropriate emission filters and a 40 ×/1.0 objective (Plan-Apochromat 40 ×/1.3 Oil DIC M27 ($a = 0.21$ mm), (UV)VIS-IR). Z-Stacks of images for expression studies were taken at 1 or 0.4 μm intervals, processed with Fiji and displayed as maximum intensity projections. 3D-visualization of z-stacks was obtained using Imaris Viewer (© Oxford Instruments). Confocal and stimulated emission depletion (STED) images were acquired on a commercial STED microscope (Abberior Instruments, Göttingen, Germany). Images were recorded with a 100X silicon oil immersion objective (NA 1.40; Olympus UPLSAPO 100XS), excitation wavelengths 485 and 640 nm, detection windows 498–520 and 650–720 nm, pixel size 20 nm, dwell time 10 μs, pinhole size 1.21 Airy Units. A STED beam of 775 nm was used. Images were linearly deconvolved (Wiener filtered) with Matlab (Mathworks, Natick, MA) using a theoretical point spread function and processed in the Inspector data acquisition and analysis environment (Abberior Instruments, Göttingen, Germany).

For quantitative analysis z-stacks of images were recorded at 0.4 μm intervals and processed with ImageJ. Mean values of regions-of-interest (ROIs) containing the nuclear signals of three consecutive z-layers, identified by TO-PRO-3 fluorescence, were determined. The quantification of nuclear H2A.Z average fluorescence intensity was calculated using the ZEN Blue Software on single planes with clear nuclear delimitation and normalized on background average fluorescence intensity. For statistical analysis GraphPad Prism 7 (GraphPad Software Inc., La Jolla CA) was used. Data sets were tested for normality using the Shapiro–Wilk normality test and the ROUT-test for outlier (significant outliers were not included in the calculation).

2.14 | Quantification and statistical analysis

Statistical analysis of the sequencing data was done in R (R Development Core Team, 2008) using the packages and functions stated in the respective analysis section. The most variable CpGs were retrieved by ordering the squared loadings of the PCA object. The distribution difference in Figure 2(a), (b) were tested with Wilcoxon rank sum test using the *wilcox.test* function. The enrichment of GO Terms was calculated using DAVID (Huang et al., 2009a, 2009b) with a p -value cut off of ≤ 0.01 .

Immunofluorescence data were analyzed with the Mann–Whitney- U -test with the following p -values $*p = .01$ – $.05$, $**p = .001$ – $.01$, $***p = .0001$ – $.001$, $****p < .00001$. Data are represented as means \pm SD of single cell values, unless otherwise stated.

3 | RESULTS

3.1 | Astrocytes from cerebellum and cortex share a basic transcriptional and epigenomic program

To characterize the molecular programs of astroglial populations from cerebral cortex (CTX) and cerebellum (CB) by an integrated



epigenomics approach, we isolated cells from young adult (6 weeks old) mice by Fluorescence Activated Cell Sorting (FACS) using the well-established hGFAP-EGFP reporter mouse line (Nolte et al., 2001). For simplicity, we will use the term CB astrocytes to describe the mixture of cerebellar astroglia largely composed of radial Bergmann glia, few astrocytes of the granular layer and cerebellar white matter (Figure S1(a)) and CTX astrocytes for the mainly protoplasmatic population isolated from the cortex. For CTX and CB fractions comparative sets of replicate libraries were constructed to monitor gene expression by mRNA-Seq, genome-wide DNA methylation by Reduced Representation Bisulfite Sequencing (RRBS) and open chromatin sites by Assay for Transposase-Accessible Chromatin (ATAC-Seq; Figure 1(a)). Libraries were sequenced on a HiSeq2500 and data were processed using DEEP pipelines (Ebert, 2016; Table S1). For additional comparisons, we performed RRBS and ATAC-Seq on FACS-sorted NeuN⁺ and NeuN⁻ nuclei fractions from the forebrain and performed RRBS on FACS sorted oligodendrocytes (PLP-DsRed1 positive cells, see Section 2.3 for more details).

To confirm the quality and purity of EGFP-positive cells, we first compared their transcriptomes to publicly available gene expression data of astrocytes isolated by other methods (Boisvert et al., 2018; Zhang et al., 2014). A principal component analyses (PCA) of the combined data revealed that astrocytes in this study were most similar to cortical astrocytes and most distant to microglia, endothelial cells and oligodendrocytes isolated from FACS sorted Aldh111⁺ cells (Figure 1(b); Zhang et al., 2014). The relative distance to astrocytes of the Boisvert study can be explained by the main technical differences in data generation. Boisvert and colleagues used astrocyte-specific Cre-mediated ribosome-tagging to isolate astroglial mRNA. Since a PCA is strongly driven by technical variations as well as by transgenic modifications of the mouse line, we also correlated gene expression levels of all data sets. Despite the technical differences and other data processing procedures, we observed an overall high correlation to all astrocyte datasets and a low correlation to other cell types (Figure S1(b), red box). In addition, we examined our transcriptome data for molecular signatures typical for astrocytes, microglia, endothelium, neurons, oligodendrocyte, or oligodendrocyte precursor cells (OPCs). Typical signatures for endothelium, neurons, and microglia were absent but we detected traces of oligodendroglial and OPC marker expression (Figure S1(c)). We assigned this to a minor contamination of floating, highly transcribed, oligodendroglial mRNAs (e.g., *Mag* and *Mog*) which is a common side effect of brain cell dissociation (Clarke et al., 2018; Krishnaswami et al., 2016; Zeisel et al., 2018) and a weak GFAP-EGFP transgene activity in some OPCs of young adult mice. We concluded that the reporter-based isolation generated highly pure astrocyte populations of CTX and CB, allowing us to perform a cell type-specific integrated epigenome and transcriptome analysis.

We next examined the genome-wide variation of DNA methylation and open chromatin between astrocyte populations and other brain derived cell types. The PCA clearly separated astrocytes from NeuN⁻, NeuN⁺ cell populations, and oligodendrocytes in the first major principal component (Figure 1(b); PC1, explaining 33% of the variance of DNA methylation and 84% of variance for open chromatin

sites). When we examined the methylation of the most variable CpGs contributing to this separation, we found clearly lower methylation in CTX and CB astrocytes compared to other cell types (Figure S1(d), left PC1). The cell type-specific epigenetic program differences of astrocytes and other cell types became most evident when we analyzed the epigenomic changes around astrocyte-specific marker genes such as *Aldh111*, *Slc1a3*, and *Gfap* (Figures S1(e), (f)). All three genes showed a cell type-specific low methylation at regulatory elements, while the promoters of neuron-specific *Tubb3* and oligodendrocyte-specific *Mag* were highly and specifically methylated in astrocytes (Figure S1(g)). Moreover, all cell type-specific DNA methylation signatures matched locus-specific open or closed chromatin states.

This indicated that astrocytes from CTX and CB share a broad spectrum of epigenomic signatures distinguishing them from non-astroglial cells. In fact, CB and CTX astrocytes shared a broad spectrum of 20,648 open chromatin regions. For these open chromatin regions, we observed a significant enrichment for CCCTC-binding factor (Ctcf) binding sites (3.6%, $p = 1e-413$) and for binding sites of the nuclear factor 1 (Nfi) family (24%, $p = 1e-188$, see Figure S1(h)). Nfia, Nfib, and Nfix are essential factors for astroglial differentiation by regulating the expression of astrocyte-specific genes. Nfia is involved in DNA-demethylation of gliogenic gene promoters such as *Gfap* and *Olig1* and promotes the transition from neurogenesis to gliogenesis in radial glia (Namihira et al., 2009; Sanosaka et al., 2017).

3.2 | Astrocytes from cerebellum and cortex differ in epigenomic and transcriptomic properties

Our first comparative analyses indicated widespread similarities between CTX and CB astrocytes with respect to both their transcriptomic and epigenomic features. Still, the PCA of DNA methylation and open chromatin data revealed a clear separation of CTX and CB astrocytes in the second principal component (PC2 in Figure 1(b)). A closer inspection of the hierarchical clustering based on the CpGs contributing to PC2 separation showed that the methylation state of CB astrocytes appeared to be closer to neurons than to CTX astrocytes, while NeuN⁻ cells and oligodendrocytes were equidistant to CB and CTX astrocytes (Figure S1d PC2). In addition, we observed that the CpGs contributing to PC2 were rather hypomethylated in CTX astrocytes compared to CB. Moreover, a genome-wide DNA methylation segmentation analysis (as described by Salhab et al., 2018, see Section 2.9), classifying the genome into highly and partially methylated domains (reflecting A/B compartments), separated CTX and CB showing that both astroglial populations slightly differ in the genome-wide methylome organization (Figure S1(i)). Finally, unsupervised hierarchical clustering of the total mRNA-Seq, ATAC-Seq, and RRBS datasets clearly separated CTX and CB astrocytes demonstrating cell type-specific differences in both, transcriptomic and epigenomic programs (Figure 1(c)).

In order to specify the observed differences in the epigenomes and transcriptomes we performed differential analyses (Figure 1(d)–(g); Table S2; see Sections 2.7–2.9 for more details on differential analyses).

We identified a total of 5363 differentially methylated regions (DMRs; 1 kb regions with at least 25% methylation difference and a q -value $\leq .01$), 3104 differentially expressed genes (DEGs; p -value $\leq .01$ and FDR $\leq .05$) and 17,097 differentially accessible regions (DARs; p -value $\leq .01$ and FDR $\leq .05$), between CTX and CB astrocytes. Inspecting the DEGs for the top differentially expressed genes we found the transcription factor (TF) genes *Lhx2*, *Emx2*, and *Foxg1* among the genes with highest fold change in expression in CTX astrocytes. In CB astrocytes we found *Dao*, encoding D-amino acid oxidase, *Slco4a1*, a sodium-independent organic anion transporter, and *Cnpy1*, the FGF signaling regulator 1, as genes with the highest fold change in expression (Table S2). The main biological processes associated with genes differentially expressed between CB and CTX astrocytes are related to ion transport, metabolism, cytoskeleton organization, glial morphogenesis, and signaling (Figure S1(j)).

For DARs, we observed that the number was approximately 12-fold higher in CTX (15,806) compared to CB astrocytes (1231; Figure 1(d), (g)). In addition, the peak height and width of open chromatin sites were more pronounced in CTX (Figure 1(g), lower panel). This indicated a major difference in local chromatin compaction and/or chromatin organization. We therefore inspected the expression of genes associated with nucleosome assembly and chromatin organization and found an enhanced expression of chromatin modifiers (*Hat1*, *Prmt2*, and *Ino80c*), telomere control and chromatin compaction genes (*Hgmb1*, *Hmgn1*), replication-independent histone variants and histone chaperones (*Anp32e*, *Npm1*, *Nap1l1*, and *Asf1a*) as well as the major members of the cohesion complex (*Smc3*, *Stag1*, *Rad21*, and *Ctcf*) in CB astrocytes (Figure 1(h)). Moreover, we identified an enhanced expression of core histone variants H2A, H2B, and H4, as well as the linker histone H1 in the cerebellum. Immunohistochemistry for H3K27me3 and H3K27ac revealed on protein level that both heterochromatic and euchromatic signatures were more prominent in CB suggesting an overall different and more densely compacted chromatin structure in CB (Figure S2(a)). This finding is contrasted by immunodetection of the histone variant H2A.Z (Figures S2(b)–(e)). H2A.Z signals were significantly more enriched in nuclei of cortical astrocytes. H2A.Z is an important variant of core histones associated with regions controlling both active and repressive gene regulation (Bargaje et al., 2012; Rege et al., 2015). Hence, the enriched signal of H2A.Z in cortical astrocytes could be interpreted as a sign of more complex overall regulatory diversity and plasticity. Along this line we observed that histone modifiers *Hdac7* and *Hdac11*, *Kmt5a*, and *Kdm5b* were stronger expressed in CTX astrocytes. We analyzed the expression pattern of these genes in recently published single cell and bulk transcriptome data sets of cerebellar or cortical astrocytes and found similar expression patterns (data not shown; Boisvert et al., 2018; Zeisel et al., 2018). For CTX astrocytes, we noticed that the 12-fold increase in open chromatin sites was not associated with a major general increase of gene expression (Figure 1(e)). Furthermore, number, size, and relative genomic distribution of DMRs was rather balanced between CB and CTX astrocytes (Figure 1(f)). In line with this observation, we found that genes associated with DNA methylation dynamics or maintenance such as *Dnmts*, *Tets*, or *MeCP2* were not differentially expressed (data not shown). We

conclude that despite of a similar range of gene activity the overall chromatin structure and in particular the number of open chromatin sites are remarkably distinct between astrocytes of the CB and CTX.

3.3 | Correlation between epigenetics and gene expression reveals coordinated regulation of cell type-specific expression

To better understand the differences in local chromatin structuring we first analyzed the relationship between open chromatin and local DNA-methylation signatures (Figures S2(f)–(j)). Loci with a higher chromatin accessibility tend to exhibit an overall lower DNA methylation in the respective astrocyte groups (Figure 2(a)). Conversely, when we investigated regions with a lower mean methylation in CB or CTX astrocytes we found a higher median DNA accessibility in the respective cell population in addition to a slightly higher expression of the associated genes (Figure 2(b)). This relation indicates that a cell type-specific openness at regulatory regions, such as potential enhancers, is accompanied by a cell type-specific methylation and transcription.

To better understand the relation between open chromatin (DARs), DNA methylation status (DMRs), and expression changes (DEGs) we performed a set of comparative tests. Relating significant DNA methylation changes to significant gene expression changes we detected 467 lower methylated regions linked to higher expression of the associated genes in CTX and 529 of such associations in CB (Figure 2(c), red boxes). In contrast to the rather equal distribution of epigenetic associations through DNA methylation in both, CTX and CB astrocytes, we observed that the link between higher chromatin accessibility and higher gene expression in CTX (3647 genes) is 10-fold higher as compared to CB (348 genes; Figure 2(d), red boxes).

We also found several cases in which gene expression was associated to DMRs and DARs in a noncanonical correlation (Figure 2(c), (d), blue boxes). We identify 328 DMRs, showing higher methylation in CTX astrocytes, were associated with higher gene expression, while 145 DMRs followed this correlation in CB astrocytes (Figure 2(c), blue boxes). Please note, that by conventional RRBS a methylated cytosine (5-mC) cannot be distinguished from its' oxidized form 5-hydroxymethyl cytosine (5-hmC). This means that a methylated cytosine could also represent a 5-hmC position. In contrast to 5-mC, 5-hmC is associated with gene activation and transcription (Wen et al., 2014; Wen & Tang, 2014). Therefore, these noncanonical observations could also reflect active gene transcription in the presence of 5-hmC.

The noncanonical correlation effect was again more prominent for DARs. Less accessible chromatin was associated with 1071 genes showing higher gene expression in CTX (Figure 2(d), blue boxes) while only 59 genes followed this association in CB. A third cross comparison between methylation and open chromatin showed that 383 DMRs overlapping with DARs had a lower methylation and increased accessibility in CTX, while only 76 DMRs overlapping with DARs followed this trend in CB astrocytes (Figure 2(e)). In summary, these three cross comparisons suggest that astrocytes of the cortex have a more widespread, variable, and diverse epigenetic control of gene expression compared

to cerebellar astrocytes. The two directions of associations between DMRs, DARs, and gene expression indicate that epigenetically marked regions are acting as potential positive or negative gene regulators for cell type-specific expression in CB and CTX cells, respectively.

3.4 | Epigenetic changes and transcription factor control

More than 90% of the DMRs and DARs identified by our analysis were located in intronic and intergenic regions (Figure 1(f), (g)), most

likely demarcating proximal and distal gene regulatory elements. To further investigate the interplay between DARs, DMRs, and astrocyte-specific transcriptional gene regulation, we performed a TF binding motif analysis on DARs and DMRs. We found that stronger enriched open chromatin regions in CTX were particularly enriched for binding sites of the TFs Lhx2 and Emx2 (Figure 3(a)). Both TFs are essential for the cerebral cortex regionalization and development (Bulchand, Grove, Porter, & Tole, 2001; Mallamaci et al., 2000). Both were among the top differentially expressed genes with an almost 250-fold stronger expression of *Lhx2* in CTX (Figure 3(e)). In addition, Lhx2/Emx2 motif-containing peaks were strongly hypomethylated in

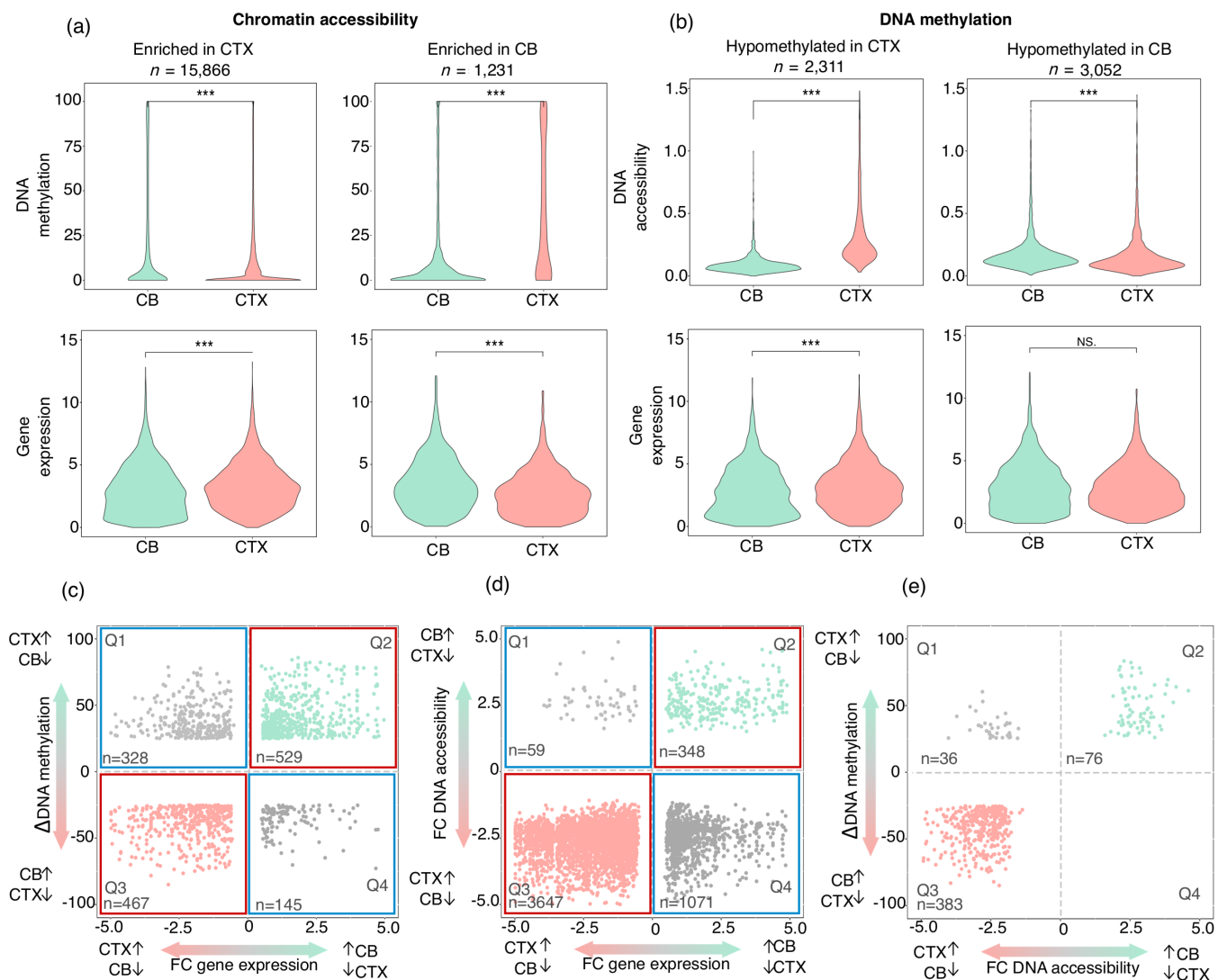


FIGURE 2 Integrating epigenetics and gene expression reveals positive and negative regulation of cell type-specific expression.

(a) Distribution of DNA methylation levels at DARs (top) and transcription of DAR-associated genes (bottom). Left for more open regions in CTX astrocytes and right for more open regions in CB astrocytes. (b) Distribution of DNA accessibility at DMRs (top) and the gene expression of DMR-associated genes (bottom). Left for hypomethylated regions in CTX astrocytes and right for hypomethylated regions in CB astrocytes. (c) Pairwise comparison of DNA methylation and gene expression differences. (d) Pairwise comparison of DNA accessibility and gene expression differences. (e) Pairwise comparison of DNA methylation and DNA accessibility differences. Positive expression FCs represent significantly higher expression or higher DNA accessibility in CB astrocytes. Negative expression FCs represent significantly higher expression or higher DNA accessibility in CTX astrocytes. Positive methylation difference represents significantly lower methylation in CB. Negative methylation difference represents significantly lower methylation in CTX astrocytes. *** $p < .001$; FC, fold change; NS, not significant (Wilcoxon Test). Data represented as mean [Color figure can be viewed at wileyonlinelibrary.com]

CTX astrocytes (Figure 3(b)). Lhx2 expression in telencephalon astrocytes was confirmed using published single cell expression data (Figure S3(c), Zeisel et al., 2018). Lhx2 protein expression in astrocytes was verified by immunohistochemistry showing a higher expression in CTX compared to CB (Figure S3b). Both, the enrichment of binding sites at open regions and the expression of Lhx2 itself suggests an important role of Lhx2 in cortical astrocytes. In CB astrocytes we found that more open chromatin regions are enriched for Zic family binding sites (Figure 3(a)). The development of a cerebellar neuron population, granule cells, was shown to be associated with DARs enriched for Zic binding at enhancers to establish gene expression patterns of mature neurons (Frank et al., 2015). However, the function of Zic proteins in cerebellar astrocytes has not been investigated so far. Along with the Zic binding prediction at specific open chromatin sites in CB, we found a strongly enhanced expression of Zic1 (63-fold), Zic2 (4-fold), and Zic4 (120-fold) and hypomethylation of the respective sites (Table S2; Figure 3(b), (e)). Published single cell expression data confirmed that Zic1 is highly expressed in nearly every Bergmann glia cell (Figure S3(c)). Immunohistochemistry of Zic1 revealed a weak protein expression in Bergmann Glia along with strong signals in Purkinje cells and granule cells, but no signals in cortical astrocytes (Figure S3(b)). The apparently prominent role of Zic family TFs in maintenance and control of cerebellar astrocytes, however, remains to be clarified.

Our motif enrichment analysis also highlighted a strong enrichment of Nfi binding motifs in regions more open in either CTX or CB astrocytes, confirming Nfi as an important astrocyte signature. Together with the strong enrichment of Nfi binding sites at nondifferential open chromatin sites (Figure S1(h)) this suggests a transcriptional control of astrocyte-specific functions but also region-specific control. In line with this, Huang and colleagues showed recently that the deletion of Nfia in adult astrocytes resulted in region-specific alterations regarding morphology and physiology of astrocytes (Huang, Woo, et al., 2020).

For motif analyses of DMRs we selected regions with a methylation difference of at least 50% between CTX and CB astrocytes reasoning that this would identify major contributions to region-specific programs. Three hundred seventy-nine of these DMRs were hypomethylated in CTX and 573 hypomethylated in CB. Interestingly, this confirmed that the strongest enrichment of Lhx2/Pou4f2/ Hoxa5 consensus motifs can be found in hypomethylated regions of the CTX (Figure 3(c)) together with significant enrichment of open chromatin at these DMRs (Figure 3(d)), while binding motifs for Sox2/Sox3/ FoxJ3 were associated with DMRs hypomethylated in CB (Figure 3(c)).

We next compared our ATAC-Seq data with published Lhx2 Chromatin Immunoprecipitation Sequencing (ChIP-Seq) data from late stage Retinal Precursor Cells (RPCs; Zibetti et al., 2019). In late-stage RPCs, Lhx2 is essential for generation of the retina-specific astrocyte-like glia called Müller glia (de Melo, Clark, et al., 2016; de Melo, Zibetti, et al., 2016) and we therefore used this data to infer actual Lhx2 binding in cortical astrocytes. We first looked at the Lhx2 enrichment across DARs and observed a strong signal of RPCs Lhx2 binding at

more open regions in cortical astrocytes (Figure S3d). We then investigated the link between differential gene expression and Lhx2 binding and extracted all Lhx2 ChIP-Seq peaks and all cortical ATAC-Seq peaks that were annotated to the identified DEGs (Figure 3(f)). We found 1044 loci to be open in CTX astrocytes and to be enriched for Lhx2. Motif enrichment analysis of these loci identified Lhx2 as the most significant motif. Of note, Lhx2 was found as the most significant motif in Lhx2 peaks that were not overlapping our ATAC-Seq data which validated the method we used to identify motif enrichment. The ATAC peaks that did not overlap with Lhx2 peaks showed enrichment for Sp1 motifs. Genes having Lhx2 binding sites were related to developmental processes while genes that did not have predicted Lhx2 binding sites were related to general astroglial characteristics. We therefore hypothesize that transcriptional control of developmental genes by Lhx2, maintains regional characteristics beyond cell differentiation, and maturation.

3.5 | Cortical and cerebellar astrocytes execute specific programs through complex epigenetic networks

To further unveil differential transcriptional programs in CTX and CB astrocytes, we focused on differentially expressed genes that were linked to DARs and DMRs (Figure 4(a)). A high proportion of these 661 identified genes encoded transcription factors and nuclei acid binding proteins, followed by hydrolases and receptors (Figure 4(b); Table S3). Functionally, the most prominent common feature of these genes was an enrichment for nervous system development (Figures 4(c) and S4(a)). Among the integrated CTX-specific genes we detected *Lhx2*, *Emx2* together with their interaction partners *Otx1*, the anti-sense transcript *Emx2os*, *Nr2e1*, *Sfrp1*, *Fezf2*, and *Sall1*. Similar to Lhx2, all these genes play a crucial role in the early patterning and development of the forebrain (Bulchand et al., 2001; Harrison, Nishinakamura, Jones, & Monaghan, 2012; Kimura et al., 2005; Monaghan et al., 1997; Trevant et al., 2008). Similarly, we found midbrain-hindbrain specification factors such as *En1*, *En2*, *Irx1*, *Irx2*, *Irx3*, *Irx5*, *Zic1*, and *Zic4* forming a group of higher expressed genes linked to local epigenetic control in CB astrocytes (Cheng et al., 2010; Elsen, Choi, Millen, Grinblat, & Prince, 2008; Lecaudey, Anselme, Dildrop, Rütther, & Schneider-Maunoury, 2005; Matsumoto et al., 2004). Of note, a large number of genes involved in negative regulation of transcription was found in CTX astrocytes while conversely a higher expression of genes involved in positive regulation of transcription was associated with CB astrocytes (Figures 4(c), (e) and S4(a), red framed genes).

The strong correlation between the cell type-specific expression of key TFs and their role in the epigenetic control of other regulatory proteins (Figure 4(b)) became even more evident when we further confined our analysis to 194 genes in which DMRs and DARs directly overlapped (Figure 4(d)). A cluster of higher expressed genes with hypomethylated open regions included the key TFs *Lhx2* in CTX (cluster 1) and *Zic1* in CB (cluster 5; Figure 4(d)). In addition, we identified

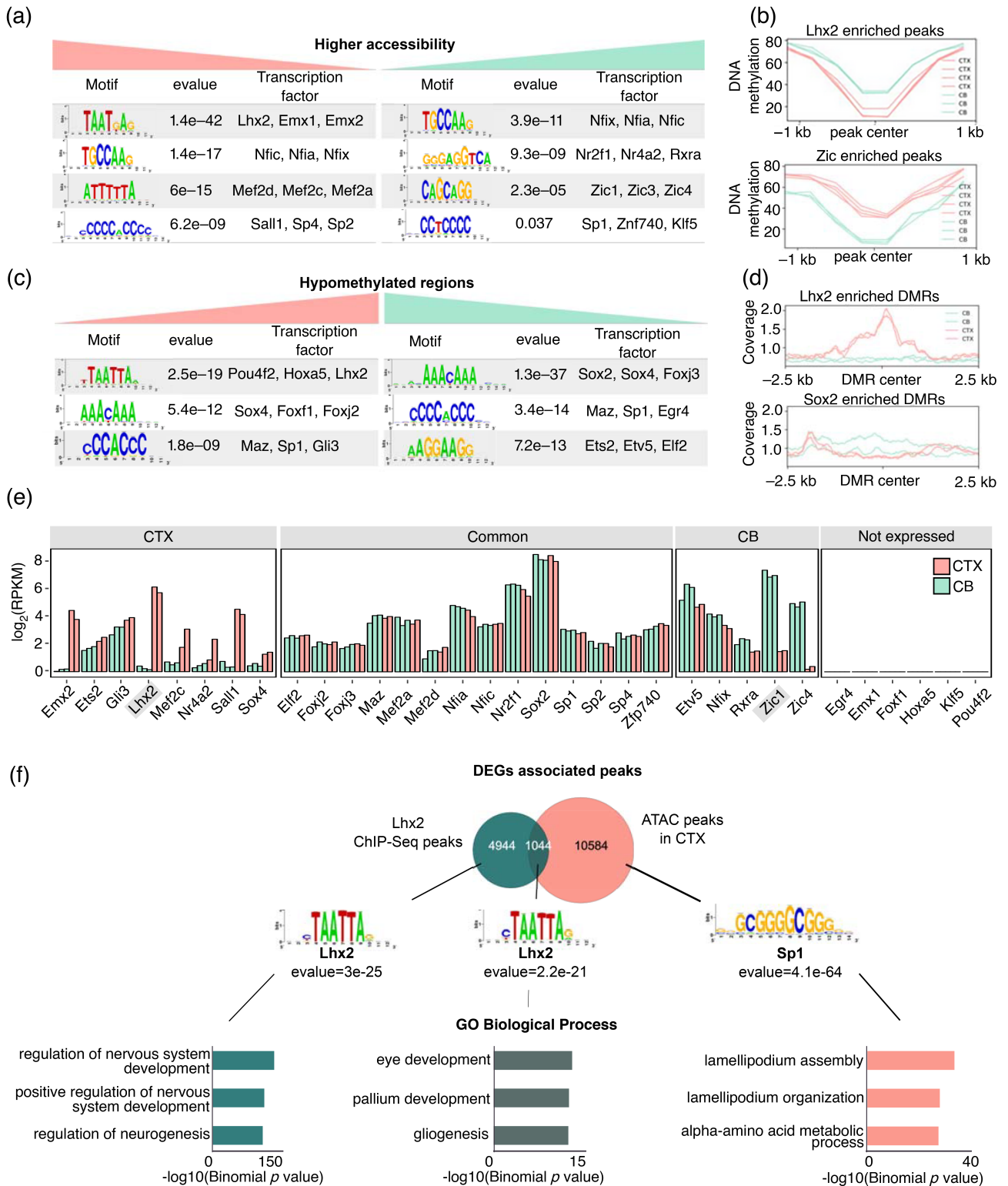


FIGURE 3 Epigenetic changes and transcription factor control. (a) Enriched transcription factor binding motifs in more accessible regions of CTX astrocytes (left) or CB astrocytes (right). (b) DNA methylation around the center of open regions (± 1 kb) enriched for Lhx2/Emx2 or Zic binding motifs. (c) Enriched transcription factor binding motifs in the hypomethylated regions of CTX astrocytes (left) or CB astrocytes (right). (d) DNA accessibility around the center of DMRs (± 2.5 kb) enriched for Lhx2 or Sox2 binding motifs. (e) Gene expression of transcription factors with enriched binding sites in DMRs or DARs grouped by higher expression in CTX astrocytes, comparable expression in both, higher expression in CB astrocytes, and not expressed. (f) Overlap of DEG associated open chromatin sites in CTX astrocytes and RPCs Lhx2 binding sites (Zibetti et al., 2019). Shown consensus sequences were the most significantly enriched motifs for respective set of peaks. In addition, the three most significant GO terms are depicted for the respective set of peaks [Color figure can be viewed at wileyonlinelibrary.com]

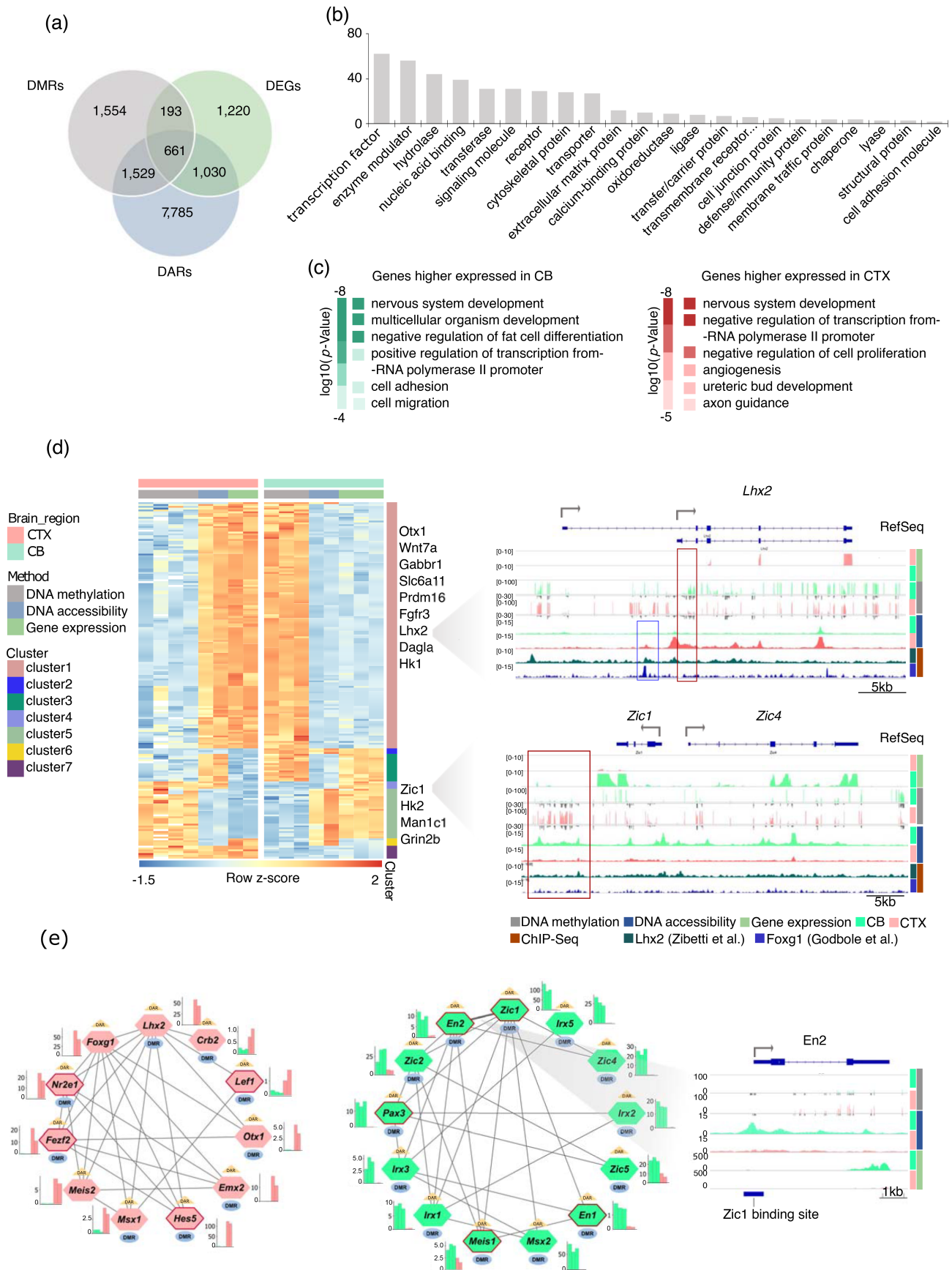


FIGURE 4 Legend on next page.

several other genes related to astrocyte-specific programs, including the membrane bound receptors *Gabbr1*, *Fgfr3*, and the metabolic genes *Dagla* and *Hk1* (cluster1) in CTX, as well as the receptor *Grin2b* or the metabolic genes *Hk2* and *Man1c1* in CB (cluster5).

Finally, we investigated the epigenetic state of genes known or predicted to be linked to *Lhx2* and *Zic1* regulation suggested by the protein-protein interaction database STRING (Figure 4(e)). Nine TF genes with connections to *Lhx2* form a network showing an exclusive or predominant expression in CTX astrocytes associated with enhanced open chromatin and the presence of DMRs. For closer inspection of these genes we examined their local epigenetic signatures. In addition, we included the *Lhx2* ChIP-Seq from late stage RPCs and a *Foxg1* ChIP-Seq dataset from embryonic cortex (Godbole et al., 2018; Zibetti et al., 2019). Because transcription factor binding is highly cell type specific, we focused on transcription factor binding sites in cellular context such as open chromatin. By doing this we found several DARs that overlapped with *Lhx2* or *Foxg1* in 10 out of 11 transcription factor network genes (Figure S4(b)). This implicates that *Lhx2* and *Foxg1* regulate the gene expression of their network factors in a combinatorial manner. To identify DEGs that are potential target genes of *Lhx2* and *Foxg1*, we extracted DEG associated open chromatin sites that overlapped with a *Lhx2* or *Foxg1* binding site (Figure S4(c)). The intersection of *Lhx2* targeted and *Foxg1* targeted genes was then subdivided into genes that were higher expressed in CTX astrocytes or higher expressed in CB astrocytes. By classification of these gene sets into protein classes we saw the highest targeting prevalence for transcriptional regulators. Interestingly, this analysis predicts members of the proposed *Zic1* network to be targeted by *Lhx2* and *Foxg1*. This would mean, that these factors not only activate region-specific gene programs but also repress programs playing an important role in other brain regions. Unfortunately, there are no ChIP-Seq datasets generated from neural cells or tissue of the other network members, so similar observations were not possible for these factors. In CB astrocytes, we identified a network of 12 TFs connected to *Zic1*, all of which showed CB-specific DMRs, DARs, and CB-specific expression. This *Zic1* network comprises several members of the Iroquois homeobox containing TF family *Irx1*, *Irx2*, *Irx3*, and *Irx5*, which have been associated with brain development in fish, frog, and chicken, but were so far not discussed in the context of mouse or human brain function. The *Zic1* network also contains the known

midbrain-hindbrain regionalization TFs *Pax3* and *En2* (Nakata, Nagai, Aruga, & Mikoshiba, 1998; Sato, Sasai, & Sasai, 2005). *En2*, almost exclusively expressed in CB astrocytes, had a CB-specific accessible region around its transcription start site. This region was confirmed to be bound by *Zic1* in the whole cerebellum (Figure 4(e); Frank et al., 2015).

We conclude that the gene expression programs of CTX and CB astrocytes are strongly controlled by a complex interplay of epigenetic control and transcription factor networks established around the developmentally important TFs such as *Lhx2* and *Zic1*, which themselves are under cell type-specific epigenetic control (Figures 4(e) and S4(b), (c)).

4 | DISCUSSION

Astrocytes of different brain regions were long regarded as rather similar cells, largely based on common functions (K^+ homeostasis, glutamate uptake, and gap junctional communication), marker expression (GFAP, S100B, and glutamine synthetase) and fine structure (perisynaptic processes, glycogen deposits, contacts to blood vessels). However, the morphological differences and detailed physiological studies of protoplasmic astrocytes in grey matter, fibrous astrocytes in white matter, radial Bergmann glia (BG) in cerebellum, Müller cells in the retina, or tanyocytes at the third ventricle revealed specific functional differences (Farmer & Murai, 2017; Reichenbach, Derouiche, & Kirchhoff, 2010). A widely discussed hypothesis suggests that functional properties of regional astrocytes are mainly determined by the distinct neuronal environments, implying an instructive, and neuronal activity dependent mechanism. However, recent bulk and single cell RNA-Seq data indicate that the molecular properties of astrocytes strongly follow region- and layer-specific cues (Batiuk et al., 2020; Bayraktar et al., 2020; Boisvert et al., 2018; Borggrewe et al., 2020; Chai et al., 2017; Itoh et al., 2018; Lin et al., 2017; Morel et al., 2017; Zeisel et al., 2018).

To better understand the underlying molecular principles, we systematically compared epigenomic and transcriptomic signatures of CTX and CB astrocytes isolated from young adult mouse brains. Our transcriptomic and epigenomic comparison of CTX and CB astrocytes suggests that astrocytes of the adult mouse brain retain signatures of

FIGURE 4 Epigenetic differences of cortical and cerebellar astrocytes highlight specific programs through complex epigenetic networks. (a) Overlap of genes associated with DMR(s), genes with differential ATAC peak(s) and differential expression. (b) Classification of the 661 intersected genes (a) into protein classes. (c) Biological processes of the 661 intersected genes (a) higher expressed in CB astrocytes ($n = 255$, left) or higher expressed in CTX astrocytes ($n = 405$, right). (d) Heatmap displaying methylation changes, chromatin accessibility changes and expression changes of genes with DMR(s) that overlap with DAR(s). Z-scores were calculated for each data set separately. On the right side, data of *Lhx2* and *Zic1/4* loci are displayed as representative genes found in cluster 1 or cluster 5, respectively. The red box indicates the epigenetically different positions identified by differential analyses. Blue box marks a previously found *Foxg1* binding site in the *Lhx2* locus (Godbole et al., 2018). Bars and peaks of biological replicates are displayed as overlaid tracks for genomic browser representations. Black bars mark covered CpG position. (e) Network analysis of *Lhx2* (left) and *Zic* family members (right) using higher expressed genes in CTX or CB astrocytes, respectively. Bar diagrams display the expression values, blue circle indicates a DMR in the respective gene and a yellow triangle indicates a DAR for the respective gene. The genome browser representation shows the *En2* locus, the blue bar indicates a *Zic1* binding position in P60 cerebellum (Frank et al., 2015) [Color figure can be viewed at wileyonlinelibrary.com]

epigenetic memory of early regional radial glia specification. This interpretation is in line with fate mapping experiments demonstrating prespecified spatial diversification of astrocytes in the brain (Tsai et al., 2012). As a sign for early regionalization memory, we regard the strong expression of the transcription factors *Lhx2*, *Emx2*, and *Foxg1* and high enrichment of their binding motifs at DARs and DMRs in cortical astrocytes. Functional studies highlighted these factors to be crucial for the specification of cortical neural progenitors (Hanashima, Li, Shen, Lai, & Fishell, 2004; Molyneaux, Arlotta, Menezes, & Macklis, 2007; Monuki, Porter, & Walsh, 2001). By combining our open chromatin data of adult astrocytes with published *Lhx2* and *Foxg1* ChIP-Seq data, we detected a high prevalence for these factors to target other transcription factors. We therefore hypothesize that these factors are placed in a high position of transcriptional hierarchy orchestrating the establishment and the propagation of regional specification. Interestingly, recent work demonstrated a direct genetic link between *Foxg1* and *Lhx2*, placing *Foxg1* upstream of *Lhx2* during the development of the cortical signaling center hem (Godbole et al., 2018). A *Foxg1* binding site was identified in the *Lhx2* locus of E14.5 cortical tissue which overlaps with an enriched open region in cortical astrocytes (Figure 4(d), blue box). The cooperative function of these transcription factors in adult astrocytes has yet to be investigated in detail on a molecular level. A recent study investigated transcriptional and chromatin changes of cortical astrocyte maturation in vivo and in vitro (Lattke, Goldstone, & Guillemot, 2020; *bioRxiv* preprint). Lattke and colleagues found *Lhx2* and *Fezf2*, which are also identified as cortical factors in this study, to be involved in astrocyte maturation in the mouse cortex in vivo. To explore the function of these factors in astrocytes they performed overexpression experiments on cultured immature astrocytes and showed that the overexpression of single transcription factors (such as *Lhx2* or *Fezf2*) could induce the expression of distinct sets of genes involved in maturation but could not change the overall expression profiles. However, in the case of a synergistic overexpression of *Fezf2* together with the transcription factor *Rorb* a larger and unique set of genes was activated. In addition, they observed extensive chromatin changes after overexpression of *Lhx2* and *Rorb*. This chromatin remodeling might be a requirement for other interacting TFs such as *Fezf2* to activate the expression of their target genes. This supports our finding of a cooperative TF network around *Lhx2* in cortical astrocytes and our interpretation of its role in the establishment and maintenance of cortical astrocyte molecular profiles. However, this hypothesis has yet to be validated by cell-specific and region-specific conditional knock-out experiments employing pairs of TFs. The mechanisms by which *Lhx2* regulates gene expression appear multifaceted. In subcortical neurons *Lhx2* was shown to determine neuronal subtype identity by interaction with the nucleosome remodeling and histone deacetylase (NuRD) complex at *Fezf2* and *Sox11* loci leading to a repression of these genes (Muralidharan et al., 2017). In retinal precursor cells *Lhx2* modulates chromatin accessibility in the course of development (Zibetti et al., 2019). Further studies on *Lhx2* function in retinal progenitor cells and Müller glia development demonstrated

stage-dependent modulation of Notch signaling factors by for example, binding to a *cis*-regulatory region of the effector *Hes5* (Figures 4 (e) and S4(b); de Melo, Clark, et al., 2016; de Melo, Zibetti, et al., 2016). We identified binding sites of *Lhx2* and *Foxg1* at transcription factors higher expressed in cerebellar astrocytes. Together with a generally higher DNA accessibility in cortical astrocytes this indicates that a set of open regions is not linked to gene activation but rather repression of genes specific for other brain regions.

A series of homeobox genes, mostly described as regulators of early brain or neuronal development, such as *En2*, *Meis2*, *Pax3*, *Hopx*, *Irx1-5*, and the zinc finger family members *Zic1* and *Zic4* showed a strong and predominant expression in CB astrocytes (Agoston, Li, Haslinger, Wizenmann, & Schulte, 2012; Zweifel et al., 2018). These genes form a network based on previous functional studies. However, it is not clear how these genes interact with each other. By the presence of DARs and DMRs in all these genes we provide potential regulatory regions that can be exploited and targeted to investigate their transcriptional control.

We observed evidence for a strong role of the nuclear factor one (Nfi) family in both adult astrocyte populations. We detected a high and almost equal expression of *Nfia*, *Nfic*, and *Nfix* in CTX and CB astrocytes accompanied by a very high enrichment of Nfi binding sites in about 25% of shared and in region-specific open chromatin sites. Studies of the developing brain identified Nfi as a central factor of the onset of astroglial development (Deneen et al., 2006; Piper et al., 2010; Sanosaka et al., 2017; Tiwari et al., 2018). The overrepresentation of Nfi binding motifs in shared and region-specific DARs together with the pan-astrocyte expression of Nfi suggests a broad regulation of common astroglial programs and the regulation of cell type-specific programs through differences in epigenetic control. In line with this, recently it was shown that an astrocyte-specific knockout of *Nfia* leads to substantial changes in gene expression and astrocyte function in hippocampal astrocytes, while astrocytes from the cortex, olfactory bulb, or brainstem were less affected (Huang, Woo, et al., 2020).

We furthermore observed a functional adaptation of astrocytes to the neuronal environment reflected in expression of transmembrane receptors, ion channels, transporters, signaling molecules, and cytoskeletal proteins in CTX and CB astrocytes. Many of these genes were linked to epigenetically controlled regulation such as *Gabbr1*, encoding the subunit 1 of the GABA_B receptor, and *Slc6a11*, encoding the GABA transporter *Gat3*, which were hypomethylated, more accessible, and higher expressed in cortical astrocytes. *Grin2b*, encoding the NMDA receptor subunit 2B, was more prominently expressed in CB astrocytes and showed hypomethylation and higher accessibility at its gene locus. We hypothesize that extracellular signals are transduced to the nucleus where effectors impinge on “preset” regulatory landscapes of epigenetic control to readily activate or repress the transcription of respective neurotransmitter receptor and transporter genes. Our findings and interpretations are supported by previous data which either focused on astrocyte (layer) heterogeneity in CTX or in CB, respectively (Farmer et al., 2016; Lanjakornsiripan et al., 2018).

A striking observation was to find a strong difference of chromatin openness around DARs of astrocytes from CTX and CB. By investigating published single cell transcriptome data (Zeisel et al., 2018), we observed that Bergman glia are represented by a dense cluster in a T-distributed Stochastic Neighbor Embedding (t-SNE) plot, while astrocytes from the telencephalon are more dispersed (Figure S3c). This suggests that CTX astrocytes execute a broader spectrum of individual gene expression programs. Their more open chromatin/less dense nucleosome structure may reflect their responsiveness to position and local environmental signals allowing a local regulatory adaptation. A recent study shows that astrocytes from the cortex are more prone to neuronal reprogramming as those from cerebellum (Hu et al., 2019). The basis for these differences may lie in the distinct TF programs but also the more open and easier reprogrammable chromatin structure of cortical astrocytes. In the cerebellum the higher expression of core histones and histone chaperones (on the transcriptional level) suggests a higher density of nucleosomes particularly around DARs. Epigenetic modifications characteristic for open chromatin at enhancers such as H3K27ac and for closed chromatin by the PRC2 mediated H3K27me3 modification are both more prominent in CB (as observed by immunohistochemistry). The genes of the PRC2 complex and the H3K27ac associated CBP/EP300 complex are expressed at the same level in both CB and CTX (data not shown). Together, these observations indicate that an overall higher nucleosome positioning and density in CB for example, around regulatory elements, is reflected in higher signal intensities of these (usually) gene specific focal modifications.

In summary, our findings suggest that key regulators, primarily identified as developmental and spatio-temporal specifiers (mainly for neurogenesis), are also prominent and persistent actors in astrocytes. Their function seems to be embedded into layers of transcriptional and epigenomic control with regional and spatial specificities for astrocytes of the cortex and the cerebellum. These observations raise the question how distinct functionalities are implemented? We are tempted to speculate that the specification into cortical and cerebellar astrocytes is a result from a combination of developmental and spatially determined epigenomic programs. Starting from an epigenetic preformation in regional common neural precursors, the final (regional) programs are overlaid or modulated by a spatial neural circuit interaction between astrocytes and neurons. This concept raises questions how and when the chromatin differences are established and how developmental regulators such as Nfi, Lhx2, or Zic1 are targeted and programmed to execute both shared and unique programs in different astrocyte types? How distinct is the gene regulation by those factors in neurons compared to astrocytes and how far do those factors regulate genes with complementary functions to ensure regionally matched interactions? Further studies combining bulk (on sorted cells) and single cell transcriptomics, bulk and single cell epigenomics with mouse genetics and physiological analysis will pave the way to gradually disentangle these programmatic changes and extend the understanding of processes in distinct neural circuits and neural circuit related diseases.

ACKNOWLEDGMENTS

Funding was provided by German Epigenome Programme (DEEP) grant (01KU1216F) by the Federal Ministry of Education and Research in Germany (BMBF). Karl Nordström was also supported by the BMBF grant for de.NBI (031L0101D) and is currently employed by AstraZeneca. This work was supported by grants of the Deutsche Forschungsgemeinschaft DFG SFB 894, SPP 1757, and ERANET Neuron (BrIE) to Frank Kirchhoff. Fluorescence activated cell sorting was performed with equipment of the FACS facility, Department of Cellular Neurophysiology, CIPMM, University of Saarland. The authors thank Konstantin Lepikhov for providing F1(C57BL6/J x DBA2/N) mouse brains. The authors thank Marcel Lauterbach and Ahmad Lotfinia for the support on STED microscopy. Open Access funding enabled and organized by Projekt DEAL.

CONFLICT OF INTEREST

The authors declare no competing interests.

AUTHOR CONTRIBUTIONS

Jörn Walter, Frank Kirchhoff, Anja Scheller, Gilles Gasparoni, Anna Welle, and Carmen V. Kasakow: Conceptualization. **Anna Welle and Carmen V. Kasakow:** Methodology. **Anna Welle, Annemarie M. Jungmann, Karl Nordström, and Abdulrahman Salhab:** Formal Analysis; **Anna Welle, Gilles Gasparoni, Carmen V. Kasakow, Davide Gobbo and Laura Stopper:** Investigation; **Anja Scheller and Frank Kirchhoff:** Resources; **Anna Welle and Jörn Walter:** Writing –Original Draft; **Anna Welle, Annemarie M. Jungmann, Carmen V. Kasakow, Davide Gobbo, Laura Stopper, and Abdulrahman Salhab:** Visualization; **Jörn Walter, Frank Kirchhoff, and Anja Scheller:** Supervision; **Jörn Walter and Frank Kirchhoff:** Funding Acquisition.

DATA AVAILABILITY STATEMENT

These sequence data have been submitted to the ENA database under accession number PRJEB31136.

ORCID

Anna Welle  <https://orcid.org/0000-0001-9915-2845>

Annemarie M. Jungmann  <https://orcid.org/0000-0003-0236-2112>

Davide Gobbo  <https://orcid.org/0000-0002-4076-2697>

Karl Nordström  <https://orcid.org/0000-0001-6231-4417>

Abdulrahman Salhab  <https://orcid.org/0000-0002-9649-6922>

Gilles Gasparoni  <https://orcid.org/0000-0002-6423-4637>

Anja Scheller  <https://orcid.org/0000-0001-8955-2634>

Frank Kirchhoff  <https://orcid.org/0000-0002-2324-2761>

Jörn Walter  <https://orcid.org/0000-0003-0563-7417>

REFERENCES

- Afgan, E., Baker, D., Batut, B., van den Beek, M., Bouvier, D., Čech, M., ... Blankenberg, D. (2018). The galaxy platform for accessible, reproducible and collaborative biomedical analyses: 2018 update. *Nucleic Acids Research*, 46(W1), W537–W544. <https://doi.org/10.1093/nar/gky379>
- Agoston, Z., Li, N., Haslinger, A., Wizenmann, A., & Schulte, D. (2012). Genetic and physical interaction of Meis2, Pax3 and Pax7 during

- dorsal midbrain development. *BMC Developmental Biology*, 12(1), 10. <https://doi.org/10.1186/1471-213X-12-10>
- Akalin, A., Kormaksson, M., Li, S., Garrett-Bakelman, F. E., Figueroa, M. E., Melnick, A., & Mason, C. E. (2012). methylKit: A comprehensive R package for the analysis of genome-wide DNA methylation profiles. *Genome Biology*, 13(10), R87. <https://doi.org/10.1186/gb-2012-13-10-r87>
- Bai, X., Saab, A. S., Huang, W., Hoberg, I. K., Kirchoff, F., & Scheller, A. (2013). Genetic background affects human glial fibrillary acidic protein promoter activity. *PLoS One*, 8(6), e66873. <https://doi.org/10.1371/journal.pone.0066873>
- Bargaje, R., Alam, M. P., Patowary, A., Sarkar, M., Ali, T., Gupta, S., ... Pillai, B. (2012). Proximity of H2A.Z containing nucleosome to the transcription start site influences gene expression levels in the mammalian liver and brain. *Nucleic Acids Research*, 40(18), 8965–8978. <https://doi.org/10.1093/nar/gks665>
- Batiuk, M. Y., Martirosyan, A., Wahis, J., de Vin, F., Marneffe, C., Kusserow, C., ... Holt, M. G. (2020). Identification of region-specific astrocyte subtypes at single cell resolution. *Nature Communications*, 11(1), 1220. <https://doi.org/10.1038/s41467-019-14198-8>
- Bayraktar, O. A., Bartels, T., Holmqvist, S., Kleshchevnikov, V., Martirosyan, A., Polioudakis, D., ... Rowitch, D. H. (2020). Astrocyte layers in the mammalian cerebral cortex revealed by a single-cell in situ transcriptomic map. *Nature Neuroscience*, 23(4), 500–509. <https://doi.org/10.1038/s41593-020-0602-1>
- Boisvert, M. M., Erikson, G. A., Shokhiev, M. N., & Allen, N. J. (2018). The aging astrocyte Transcriptome from multiple regions of the mouse brain. *Cell Reports*, 22(1), 269–285. <https://doi.org/10.1016/j.celrep.2017.12.039>
- Borggrewe, M., Grit, C., Vainchtein, I. D., Brouwer, N., Wesseling, E. M., Laman, J. D., ... Boddeke, E. W. G. M. (2020). Regionally diverse astrocyte subtypes and their heterogeneous response to EAE. *Glia*, 69, 1140–1154. <https://doi.org/10.1002/glia.23954>
- Bulchand, S., Grove, E. A., Porter, F. D., & Tole, S. (2001). LIM-homeodomain gene Lhx2 regulates the formation of the cortical hem. *Mechanisms of Development*, 100(2), 165–175. [https://doi.org/10.1016/S0925-4773\(00\)00515-3](https://doi.org/10.1016/S0925-4773(00)00515-3)
- Burger, L., Gaidatzis, D., Schübeler, D., & Stadler, M. B. (2013). Identification of active regulatory regions from DNA methylation data. *Nucleic Acids Research*, 41(16), e155–e155. <https://doi.org/10.1093/nar/gkt599>
- Chai, H., Diaz-Castro, B., Shigetomi, E., Monte, E., Oceau, J. C., Yu, X., ... Khakh, B. S. (2017). Neural circuit-specialized astrocytes: transcriptomic, proteomic, morphological, and functional evidence. *Neuron*, 95(3), 531–549. <https://doi.org/10.1016/j.neuron.2017.06.029>
- Chen, T.-W., Li, H.-P., Lee, C.-C., Gan, R.-C., Huang, P.-J., Wu, T. H., ... Tang, P. (2014). ChIPseeker, a web-based analysis tool for ChIP data. *BMC Genomics*, 15(1), 539. <https://doi.org/10.1186/1471-2164-15-539>
- Cheng, Y., Sudarov, A., Szulc, K. U., Sgaier, S. K., Stephen, D., Turnbull, D. H., & Joyner, A. L. (2010). The engrailed homeobox genes determine the different foliation patterns in the vermis and hemispheres of the mammalian cerebellum. *Development*, 137(3), 519–529. <https://doi.org/10.1242/dev.027045>
- Clarke, B. E., Taha, D. M., Tyzack, G. E., & Patani, R. (2021). Regionally encoded functional heterogeneity of astrocytes in health and disease: A perspective. *Glia*, 69(1), 20–27. <https://doi.org/10.1002/glia.23877>
- Clarke, L. E., Liddelov, S. A., Chakraborty, C., Münch, A. E., Heiman, M., & Barres, B. A. (2018). Normal aging induces A1-like astrocyte reactivity. *Proceedings of the National Academy of Sciences*, 115(8), E1896–E1905. <https://doi.org/10.1073/pnas.1800165115>
- de Melo, J., Clark, B. S., & Blackshaw, S. (2016). Multiple intrinsic factors act in concert with Lhx2 to direct retinal gliogenesis. *Scientific Reports*, 6, 32757. <https://doi.org/10.1038/srep32757>
- de Melo, J., Zibetti, C., Clark, B. S., Hwang, W., Miranda-Angulo, A. L., Qian, J., & Blackshaw, S. (2016). Lhx2 is an essential factor for retinal Gliogenesis and notch signaling. *The Journal of Neuroscience: The Official Journal of the Society for Neuroscience*, 36(8), 2391–2405. <https://doi.org/10.1523/JNEUROSCI.3145-15.2016>
- DeLuca, D. S., Levin, J. Z., Sivachenko, A., Fennell, T., Nazaire, M.-D., Williams, C., ... Getz, G. (2012). RNA-SeqQC: RNA-seq metrics for quality control and process optimization. *Bioinformatics*, 28(11), 1530–1532. <https://doi.org/10.1093/bioinformatics/bts196>
- Deneen, B., Ho, R., Lukaszewicz, A., Hochstim, C. J., Gronostajski, R. M., & Anderson, D. J. (2006). The transcription factor NFIA controls the onset of Gliogenesis in the developing spinal cord. *Neuron*, 52(6), 953–968. <https://doi.org/10.1016/j.neuron.2006.11.019>
- Dobin, A., & Gingeras, T. R. (2015). Mapping RNA-seq reads with STAR: Mapping RNA-seq reads with STAR. In A. Bateman, W. R. Pearson, L. D. Stein, G. D. Stormo, & J. R. Yates (Eds.), *Current protocols in bioinformatics* (pp. 11.14.1–11.14.19 (Vol. 51)). Hoboken, NJ: John Wiley & Sons, Inc.. <https://doi.org/10.1002/0471250953.bi114s51>
- Durek, P., Nordström, K., Gasparoni, G., Salhab, A., Kressler, C., de Almeida, M., ... Polansky, J. K. (2016). Epigenomic profiling of human CD4⁺ T cells supports a linear differentiation model and highlights molecular regulators of memory development. *Immunity*, 45(5), 1148–1161. <https://doi.org/10.1016/j.immuni.2016.10.022>
- Ebert, P. (2016). *Deep computational metadata*. Max Planck Institute for Informatics. <https://doi.org/10.17617/1.2W>
- Elsen, G. E., Choi, L. Y., Millen, K. J., Grinblat, Y., & Prince, V. E. (2008). Zic1 and Zic4 regulate zebrafish roof plate specification and hindbrain ventricle morphogenesis. *Developmental Biology*, 314(2), 376–392. <https://doi.org/10.1016/j.ydbio.2007.12.006>
- Farmer, W. T., & Murai, K. (2017). Resolving astrocyte heterogeneity in the CNS. *Frontiers in Cellular Neuroscience*, 11, 300. <https://doi.org/10.3389/fncel.2017.00300>
- Farmer, W. T., Abrahamsson, T., Chierzi, S., Lui, C., Zaelzer, C., Jones, E. V., ... Murai, K. K. (2016). Neurons diversify astrocytes in the adult brain through sonic hedgehog signaling. *Science*, 351(6275), 849–854. <https://doi.org/10.1126/science.aab3103>
- Frank, C. L., Liu, F., Wijayatunge, R., Song, L., Biegler, M. T., Yang, M. G., ... West, A. E. (2015). Regulation of chromatin accessibility and Zic binding at enhancers in the developing cerebellum. *Nature Neuroscience*, 18(5), 647–656. <https://doi.org/10.1038/nn.3995>
- Godbole, G., Shetty, A. S., Roy, A., D'Souza, L., Chen, B., Miyoshi, G., ... Tole, S. (2018). Hierarchical genetic interactions between FOXG1 and LHX2 regulate the formation of the cortical hem in the developing telencephalon. *Development*, 145(1), dev154583. <https://doi.org/10.1242/dev.154583>
- Hanashima, C., Li, S. C., Shen, L., Lai, E., & Fishell, G. (2004). Foxg1 suppresses early cortical cell fate. *Science*, 303(5654), 56–59. <https://doi.org/10.1126/science.1090674>
- Harrison, S. J., Nishinakamura, R., Jones, K. R., & Monaghan, A. P. (2012). Sall1 regulates cortical neurogenesis and laminar fate specification in mice: Implications for neural abnormalities in Townes-Brocks syndrome. *Disease Models & Mechanisms*, 5(3), 351–365. <https://doi.org/10.1242/dmm.002873>
- Hirrlinger, P. G., Scheller, A., Braun, C., Quintela-Schneider, M., Fuss, B., Hirrlinger, J., & Kirchhoff, F. (2005). Expression of reef coral fluorescent proteins in the central nervous system of transgenic mice. *Molecular and Cellular Neurosciences*, 30(3), 291–303. <https://doi.org/10.1016/j.mcn.2005.08.011>
- Hovestadt, V., Jones, D. T. W., Picelli, S., Wang, W., Kool, M., Northcott, P. A., ... Lichter, P. (2014). Decoding the regulatory landscape of medulloblastoma using DNA methylation sequencing. *Nature*, 510(7506), 537–541. <https://doi.org/10.1038/nature13268>
- Hu, X., Qin, S., Huang, X., Yuan, Y., Tan, Z., Gu, Y., ... Su, Z. (2019). Region-restrict astrocytes exhibit heterogeneous susceptibility to neuronal reprogramming. *Stem Cell Reports*, 12(2), 290–304. <https://doi.org/10.1016/j.stemcr.2018.12.017>



- Huang, A. Y.-S., Woo, J., Sardar, D., Lozzi, B., Bosquez Huerta, N. A., Lin, C.-C. J., ... Deneen, B. (2020). Region-specific transcriptional control of astrocyte function oversees local circuit activities. *Neuron*, 106(6), 992–1008. <https://doi.org/10.1016/j.neuron.2020.03.025>
- Huang, D. W., Sherman, B. T., & Lempicki, R. A. (2009a). Bioinformatics enrichment tools: Paths toward the comprehensive functional analysis of large gene lists. *Nucleic Acids Research*, 37(1), 1–13. <https://doi.org/10.1093/nar/gkn923>
- Huang, D. W., Sherman, B. T., & Lempicki, R. A. (2009b). Systematic and integrative analysis of large gene lists using DAVID bioinformatics resources. *Nature Protocols*, 4(1), 44–57. <https://doi.org/10.1038/nprot.2008.211>
- Huang, W., Bai, X., Meyer, E., & Scheller, A. (2020). Acute brain injuries trigger microglia as an additional source of the proteoglycan NG2. *Acta Neuropathologica Communications*, 8(1), 146. <https://doi.org/10.1186/s40478-020-01016-2>
- Itoh, N., Itoh, Y., Tassoni, A., Ren, E., Kaito, M., Ohno, A., ... Voskuhl, R. R. (2018). Cell-specific and region-specific transcriptomics in the multiple sclerosis model: Focus on astrocytes. *Proceedings of the National Academy of Sciences*, 115(2), E302–E309. <https://doi.org/10.1073/pnas.1716032115>
- Jahn, H. M., Kasakow, C. V., Helfer, A., Michely, J., Verkhatsky, A., Maurer, H. H., ... Kirchhoff, F. (2018). Refined protocols of tamoxifen injection for inducible DNA recombination in mouse astroglia. *Scientific Reports*, 8(1), 5913. <https://doi.org/10.1038/s41598-018-24085-9>
- Kimura, J., Suda, Y., Kurokawa, D., Hossain, Z. M., Nakamura, M., Takahashi, M., ... Aizawa, S. (2005). Emx2 and Pax6 function in cooperation with Otx2 and Otx1 to develop caudal forebrain primordium that includes future Archipallium. *Journal of Neuroscience*, 25(21), 5097–5108. <https://doi.org/10.1523/JNEUROSCI.0239-05.2005>
- Krishnaswami, S. R., Grindberg, R. V., Novotny, M., Venepally, P., Lacar, B., Bhutani, K., ... Lasken, R. S. (2016). Using single nuclei for RNA-seq to capture the transcriptome of postmortem neurons. *Nature Protocols*, 11(3), 499–524. <https://doi.org/10.1038/nprot.2016.015>
- Lanjakonsiripan, D., Pior, B.-J., Kawaguchi, D., Furutachi, S., Tahara, T., Katsuyama, Y., ... Gotoh, Y. (2018). Layer-specific morphological and molecular differences in neocortical astrocytes and their dependence on neuronal layers. *Nature Communications*, 9(1), 1623. <https://doi.org/10.1038/s41467-018-03940-3>
- Lattke, M., Goldstone, R., & Guillemot, F. (2020). Extensive transcriptional and chromatin changes underlie astrocyte maturation in vivo and in culture. *BioRxiv*. 2020.04.28.066043. <https://doi.org/10.1101/2020.04.28.066043>
- Lecaudey, V., Anselme, I., Dildrop, R., R  ther, U., & Schneider-Maunoury, S. (2005). Expression of the zebrafish Iroquois genes during early nervous system formation and patterning. *Journal of Comparative Neurology*, 492(3), 289–302. <https://doi.org/10.1002/cne.20765>
- Li, H., Handsaker, B., Wysoker, A., Fennell, T., Ruan, J., Homer, N., ... 1000 Genome Project Data Processing Subgroup. (2009). The sequence alignment/map format and SAMtools. *Bioinformatics*, 25(16), 2078–2079. <https://doi.org/10.1093/bioinformatics/btp352>
- Liao, Y., Smyth, G. K., & Shi, W. (2014). featureCounts: An efficient general purpose program for assigning sequence reads to genomic features. *Bioinformatics*, 30(7), 923–930. <https://doi.org/10.1093/bioinformatics/btt656>
- Lin, J. C.-C., Yu, K., Hatcher, A., Huang, T.-W., Lee, H. K., Carlson, J., ... Deneen, B. (2017). Identification of diverse astrocyte populations and their malignant analogs. *Nature Neuroscience*, 20(3), 396–405. <https://doi.org/10.1038/nn.4493>
- Lovatt, D., Sonnewald, U., Waagepetersen, H. S., Schousboe, A., He, W., Lin, J. H.-C., ... Nedergaard, M. (2007). The transcriptome and metabolic gene signature of protoplasmic astrocytes in the adult murine cortex. *Journal of Neuroscience*, 27(45), 12255–12266. <https://doi.org/10.1523/JNEUROSCI.3404-07.2007>
- Lun, A. T. L., & Smyth, G. K. (2016). Csaw: A bioconductor package for differential binding analysis of ChIP-seq data using sliding windows. *Nucleic Acids Research*, 44(5), e45. <https://doi.org/10.1093/nar/gkv1191>
- Mallamaci, A., Mercurio, S., Muzio, L., Cecchi, C., Pardini, C. L., Gruss, P., & Boncinelli, E. (2000). The lack of Emx2 causes impairment of Reelin signaling and defects of neuronal migration in the developing cerebral cortex. *The Journal of Neuroscience: The Official Journal of the Society for Neuroscience*, 20(3), 1109–1118.
- Marco-Sola, S., Sammeth, M., Guig  , R., & Ribeca, P. (2012). The GEM mapper: Fast, accurate and versatile alignment by filtration. *Nature Methods*, 9(12), 1185–1188. <https://doi.org/10.1038/nmeth.2221>
- Martin, M. (2011). Cutadapt removes adapter sequences from high-throughput sequencing reads. *EMBnet Journal*, 17(1), 10–12. <https://doi.org/10.14806/ej.17.1.200>
- Matevossian, A., & Akbarian, S. (2008). Neuronal nuclei isolation from human postmortem brain tissue. *Journal of Visualized Experiments: JoVE*, 20, e914. <https://doi.org/10.3791/914>
- Matsumoto, K., Nishihara, S., Kamimura, M., Shiraiishi, T., Otaguro, T., Uehara, M., ... Ogura, T. (2004). The prepattern transcription factor Irx2, a target of the FGF8/MAP kinase cascade, is involved in cerebellum formation. *Nature Neuroscience*, 7(6), 605–612. <https://doi.org/10.1038/nn1249>
- McLean, C. Y., Bristor, D., Hiller, M., Clarke, S. L., Schaar, B. T., Lowe, C. B., ... Bejerano, G. (2010). GREAT improves functional interpretation of cis-regulatory regions. *Nature Biotechnology*, 28(5), 495–501. <https://doi.org/10.1038/nbt.1630>
- Mi, H., Huang, X., Muruganujan, A., Tang, H., Mills, C., Kang, D., & Thomas, P. D. (2017). PANTHER version 11: Expanded annotation data from gene ontology and Reactome pathways, and data analysis tool enhancements. *Nucleic Acids Research*, 45(D1), D183–D189. <https://doi.org/10.1093/nar/gkw1138>
- Mi, H., Muruganujan, A., Casagrande, J. T., & Thomas, P. D. (2013). Large-scale gene function analysis with the PANTHER classification system. *Nature Protocols*, 8(8), 1551–1566. <https://doi.org/10.1038/nprot.2013.092>
- Molyneaux, B. J., Arlotta, P., Menezes, J. R. L., & Macklis, J. D. (2007). Neuronal subtype specification in the cerebral cortex. *Nature Reviews Neuroscience*, 8(6), 427–437. <https://doi.org/10.1038/nrn2151>
- Monaghan, A. P., Bock, D., Gass, P., Schw  ger, A., Wolfer, D. P., Lipp, H. P., & Sch  tz, G. (1997). Defective limbic system in mice lacking the taillless gene. *Nature*, 390(6659), 515–517. <https://doi.org/10.1038/37364>
- Monuki, E. S., Porter, F. D., & Walsh, C. A. (2001). Patterning of the dorsal telencephalon and cerebral cortex by a roof plate-Lhx2 pathway. *Neuron*, 32(4), 591–604. [https://doi.org/10.1016/S0896-6273\(01\)00504-9](https://doi.org/10.1016/S0896-6273(01)00504-9)
- Morel, L., Chiang, M. S. R., Higashimori, H., Shoneye, T., Iyer, L. K., Yelick, J., ... Yang, Y. (2017). Molecular and functional properties of regional astrocytes in the adult brain. *The Journal of Neuroscience*, 37(36), 8706–8717. <https://doi.org/10.1523/JNEUROSCI.3956-16.2017>
- Muralidharan, B., Khatri, Z., Maheshwari, U., Gupta, R., Roy, B., Pradhan, S. J., ... Tole, S. (2017). LHX2 interacts with the NuRD complex and regulates cortical neuron subtype determinants *Fezf2* and *Sox11*. *The Journal of Neuroscience*, 37(1), 194–203. <https://doi.org/10.1523/JNEUROSCI.2836-16.2016>
- Nakata, K., Nagai, T., Aruga, J., & Mikoshiba, K. (1998). Xenopus *Zic* family and its role in neural and neural crest development. *Mechanisms of Development*, 75(1), 43–51. [https://doi.org/10.1016/S0925-4773\(98\)00073-2](https://doi.org/10.1016/S0925-4773(98)00073-2)
- Namihira, M., Kohyama, J., Semi, K., Sanosaka, T., Deneen, B., Taga, T., & Nakashima, K. (2009). Committed neuronal precursors confer Astrocytic potential on residual neural precursor cells. *Developmental Cell*, 16(2), 245–255. <https://doi.org/10.1016/j.devcel.2008.12.014>

- Nguyen, N. T. T., Contreras-Moreira, B., Castro-Mondragon, J. A., Santana-Garcia, W., Ossio, R., Robles-Espinoza, C. D., ... Thomas-Chollier, M. (2018). RSAT 2018: Regulatory sequence analysis tools 20th anniversary. *Nucleic Acids Research*, 46(W1), W209–W214. <https://doi.org/10.1093/nar/gky317>
- Nolte, C., Matyash, M., Pivneva, T., Schipke, C. G., Ohlemeyer, C., Hanisch, U.-K., ... Kettenmann, H. (2001). GFAP promoter-controlled EGFP-expressing transgenic mice: A tool to visualize astrocytes and astrogliosis in living brain tissue. *Glia*, 33(1), 72–86. [https://doi.org/10.1002/1098-1136\(20010101\)33:1<72::AID-GLIA1007>3.0.CO;2-A](https://doi.org/10.1002/1098-1136(20010101)33:1<72::AID-GLIA1007>3.0.CO;2-A)
- Orre, M., Kamphuis, W., Osborn, L. M., Melief, J., Kooijman, L., Huitinga, I., ... Hol, E. M. (2014). Acute isolation and transcriptome characterization of cortical astrocytes and microglia from young and aged mice. *Neurobiology of Aging*, 35(1), 1–14. <https://doi.org/10.1016/j.neurobiolaging.2013.07.008>
- Piper, M., Barry, G., Hawkins, J., Mason, S., Lindwall, C., Little, E., ... Richards, L. J. (2010). NFIA controls telencephalic progenitor cell differentiation through repression of the notch effector Hes1. *The Journal of Neuroscience: The Official Journal of the Society for Neuroscience*, 30(27), 9127–9139. <https://doi.org/10.1523/JNEUROSCI.6167-09.2010>
- R Development Core Team. (2008). *R: A language and environment for statistical computing*. Vienna, Austria: R Foundation for Statistical Computing Retrieved from <http://www.R-project.org>
- Ramírez, F., Dündar, F., Diehl, S., Grüning, B. A., & Manke, T. (2014). deepTools: A flexible platform for exploring deep-sequencing data. *Nucleic Acids Research*, 42(Web Server issue), W187–W191. <https://doi.org/10.1093/nar/gku365>
- Rege, M., Subramanian, V., Zhu, C., Hsieh, T.-H. S., Weiner, A., Friedman, N., ... Peterson, C. L. (2015). Chromatin dynamics and the RNA exosome function in concert to regulate transcriptional homeostasis. *Cell Reports*, 13(8), 1610–1622. <https://doi.org/10.1016/j.celrep.2015.10.030>
- Reichenbach, A., Derouiche, A., & Kirchhoff, F. (2010). Morphology and dynamics of perisynaptic glia. *Brain Research Reviews*, 63(1–2), 11–25. <https://doi.org/10.1016/j.brainresrev.2010.02.003>
- Robinson, J. T., Thorvaldsdóttir, H., Winckler, W., Guttman, M., Lander, E. S., Getz, G., & Mesirov, J. P. (2011). Integrative genomics viewer. *Nature Biotechnology*, 29, 24–26. <https://doi.org/10.1038/nbt.1754>
- Robinson, M. D., McCarthy, D. J., & Smyth, G. K. (2010). edgeR: A bioconductor package for differential expression analysis of digital gene expression data. *Bioinformatics*, 26(1), 139–140. <https://doi.org/10.1093/bioinformatics/btp616>
- Salhab, A., Nordström, K., Gasparoni, G., Kattler, K., Ebert, P., Ramirez, F., ... Walter, J. (2018). A comprehensive analysis of 195 DNA methylomes reveals shared and cell-specific features of partially methylated domains. *Genome Biology*, 19(1), 150. <https://doi.org/10.1186/s13059-018-1510-5>
- Sanosaka, T., Imamura, T., Hamazaki, N., Chai, M., Igarashi, K., Ideta-Otsuka, M., ... Nakashima, K. (2017). DNA Methylome analysis identifies transcription factor-based Epigenomic signatures of multilineage competence in neural stem/progenitor cells. *Cell Reports*, 20(12), 2992–3003. <https://doi.org/10.1016/j.celrep.2017.08.086>
- Sato, T., Sasai, N., & Sasai, Y. (2005). Neural crest determination by co-activation of Pax3 and Zic1 genes in *Xenopus* ectoderm. *Development*, 132(10), 2355–2363. <https://doi.org/10.1242/dev.01823>
- Shannon, P., Markiel, A., Ozier, O., Baliga, N. S., Wang, J. T., Ramage, D., ... Ideker, T. (2003). Cytoscape: A software environment for integrated models of biomolecular interaction networks. *Genome Research*, 13(11), 2498–2504. <https://doi.org/10.1101/gr.1239303>
- Supek, F., Bošnjak, M., Škunca, N., & Šmuc, T. (2011). REVIGO summarizes and visualizes long lists of gene ontology terms. *PLoS One*, 6(7), e21800. <https://doi.org/10.1371/journal.pone.0021800>
- Szklarczyk, D., Morris, J. H., Cook, H., Kuhn, M., Wyder, S., Simonovic, M., ... von Mering, C. (2017). The STRING database in 2017: Quality-controlled protein-protein association networks, made broadly accessible. *Nucleic Acids Research*, 45(D1), D362–D368. <https://doi.org/10.1093/nar/gkw937>
- Thorvaldsdóttir, H., Robinson, J. T., & Mesirov, J. P. (2013). Integrative genomics viewer (IGV): High-performance genomics data visualization and exploration. *Briefings in Bioinformatics*, 14(2), 178–192. <https://doi.org/10.1093/bib/bbs017>
- Tiwari, N., Pataskar, A., Péron, S., Thakurela, S., Sahu, S. K., Figueres-Oñate, M., ... Berninger, B. (2018). Stage-specific transcription factors drive Astroglialogenesis by remodeling gene regulatory landscapes. *Cell Stem Cell*, 23(4), 557–571. <https://doi.org/10.1016/j.stem.2018.09.008>
- Trevant, B., Gaur, T., Hussain, S., Symons, J., Komm, B. S., Bodine, P. V. N., ... Lian, J. B. (2008). Expression of secreted frizzled related protein 1, a Wnt antagonist, in brain, kidney, and skeleton is dispensable for Normal embryonic development. *Journal of Cellular Physiology*, 217(1), 113–126. <https://doi.org/10.1002/jcp.21482>
- Tsai, H.-H., Li, H., Fuentealba, L. C., Molofsky, A. V., Taveira-Marques, R., Zhuang, H., ... Rowitch, D. H. (2012). Regional astrocyte allocation regulates CNS synaptogenesis and repair. *Science (New York, N.Y.)*, 337(6092), 358–362. <https://doi.org/10.1126/science.1222381>
- Wen, L., Li, X., Yan, L., Tan, Y., Li, R., Zhao, Y., ... Qiao, J. (2014). Whole-genome analysis of 5-hydroxymethylcytosine and 5-methylcytosine at base resolution in the human brain. *Genome Biology*, 15(3), R49. <https://doi.org/10.1186/gb-2014-15-3-r49>
- Wen, L., & Tang, F. (2014). Genomic distribution and possible functions of DNA hydroxymethylation in the brain. *Genomics*, 104(5), 341–346. <https://doi.org/10.1016/j.ygeno.2014.08.020>
- Zeisel, A., Hochgerner, H., Lönnerberg, P., Johnsson, A., Memic, F., van der Zwan, J., ... Linnarsson, S. (2018). Molecular architecture of the mouse nervous system. *Cell*, 174(4), 999–1014. <https://doi.org/10.1016/j.cell.2018.06.021>
- Zhang, Y., Chen, K., Sloan, S. A., Bennett, M. L., Scholze, A. R., O'Keefe, S., ... Wu, J. Q. (2014). An RNA-sequencing transcriptome and splicing database of glia, neurons, and vascular cells of the cerebral cortex. *Journal of Neuroscience*, 34(36), 11929–11947. <https://doi.org/10.1523/JNEUROSCI.1860-14.2014>
- Zhang, Y., Liu, T., Meyer, C. A., Eeckhoute, J., Johnson, D. S., Bernstein, B. E., ... Liu, X. S. (2008). Model-based analysis of ChIP-Seq (MACS). *Genome Biology*, 9(9), R137. <https://doi.org/10.1186/gb-2008-9-9-r137>
- Zibetti, C., Liu, S., Wan, J., Qian, J., & Blackshaw, S. (2019). Epigenomic profiling of retinal progenitors reveals LHX2 is required for developmental regulation of open chromatin. *Communications Biology*, 2(1), 1–13. <https://doi.org/10.1038/s42003-019-0375-9>
- Zweifel, S., Marcy, G., Lo Guidice, Q., Li, D., Heinrich, C., Azim, K., & Raineteau, O. (2018). HOPX defines heterogeneity of postnatal subventricular zone neural stem cells. *Stem Cell Reports*, 11(3), 770–783. <https://doi.org/10.1016/j.stemcr.2018.08.006>

SUPPORTING INFORMATION

Additional supporting information may be found online in the Supporting Information section at the end of this article.

How to cite this article: Welle, A., Kasakow, C. V., Jungmann, A. M., Gobbo, D., Stopper, L., Nordström, K., Salhab, A., Gasparoni, G., Scheller, A., Kirchhoff, F., & Walter, J. (2021). Epigenetic control of region-specific transcriptional programs in mouse cerebellar and cortical astrocytes. *Glia*, 69(9), 2160–2177. <https://doi.org/10.1002/glia.24016>